Title
Parametric Amplication of Time-varying Transmission Lines (TVTL) and its Applications

Author
Zou, Xiating

Publication Date
2018

Peer reviewed|Thesis/dissertation

UNIVERSITY OF CALIFORNIA

Los Angeles

Parametric Amplification of Time-varying Transmission Lines (TVTL) and its Applications

A thesis submitted in partial satisfaction

of the requirements for the degree

Master of Science in Electrical and Computer Engineering

by

Xiating Zou

2018

ABSTRACT OF THE THESIS

Parametric Amplification of Time-varying Transmission Lines (TVTL) and its Applications

by

Xiating Zou

Master of Science in Electrical and Computer Engineering

University of California, Los Angeles, 2018

Professor Yuanxun Ethan Wang, Chair

Time-varying transmission lines (TVTL) has recently been introduced as one of the most promising transmission line structures that offers non-reciprocal frequency translation without magnetic materials [1–4]. Its sinusoidal parametric amplification with almost no noise penalty has been widely discussed and applied in building components such as broadband circulator. In this research, this parametric coupling mode was applied as a parametric mixer in frequency translational RF receiver. The frequency translational RF receiver can select the desired received band in the presence of undesired adjacent-channel blockers without suffering much signal-to-noise (SNR) degradation.

Exponential parametric amplification is another parametric amplification mode in TVTL that has not yet been fully explored. It can be achieved by designing the cutoff frequency of TVTL to short-circuit the upper sideband ω_{m+s} of converted signals. Recent measurements on a 12-unit TVTL chip showed proofs of the theory of exponential parametric amplification at signal frequency ω_s. A maximum of 2.43 dB insertion loss improvement was observed at 1.2 GHz with a 21.4 dBm carrier driven at 6 GHz. Furthermore, the noise figure of TVTL in exponential amplification region was generally better than that of the passive TVTL, indicating a better noise performance with the help of exponential amplification.

The thesis of Xiating Zou is approved.

Tatsuo Itoh

Sudhakar Pamarti

Yuanxun Ethan Wang, Committee Chair

University of California, Los Angeles

2018

To mom, Jin and Juzi.

Table of Contents

List of Figures

Acknowledgment

First of all, I would like to thank my advisor Professor Yuanxun Ethan Wang for his continuous guidance and support throught my two-year study and research at UCLA. His time and attention help me overcome countless difficulties in my research and make this work possible.

I am very grateful to my lab mates Qianteng Wu, Dr. Lap K Yeung, Mathew Biedka, Dr. Shihan Qin, Dr. Qiang Xu, Dr. Rui Zhu, Dr. Jackie (Zhi) Yao, Ting Lu and Nicolas Gutierrez for their unconditional help and discussions throughout the research and the writing of this thesis.

I would also like to express my gratitude to my committee members Professor Tatsuo Itoh and Professor Sudhakar Pamarti for their attention and patience on reading and approving this work.

Last but not least, I would like to thank my mom, my boyfriend and my cat for their mental support to me. Their love and encouragement help me come through my hard time.

This work is supported by National Science Foundation under award No.1610594 and DAPAR SPAR program.

CHAPTER 1

Introduction

1.1 Challenges in Wireless Communication Systems

With the advance of modern wireless communication, people have enjoyed much convenience brought by compact handheld devices. We can talk to people that are thousands of miles away while walking on the street; we can listen to music on our way home; we can even watch a NBA game while sitting in the airport lounge. The available spectrum resource, however, has become extremely overcrowded due to these increasingly growing multimedia applications. Meanwhile, people are continuously demanding for faster data rate, smaller device size and lower money cost. These impose huge challenges on wireless communication systems.

In order to make wireless communication systems faster, more efficient, and more robust, various digital modulations such as CDMA [6] and OFDM [7] were developed. These modulations may greatly improve system performance, however, they also produce non-constant-envelope signals. These non-constant-envelope signals can spread to adjacent channels after passing nonideal transmitters [8, 9]. Adjacent channel interference can affect the signal-to-noise ratio (SNR) at receivers significantly. In addition, low-noise amplifiers in receivers may also saturate by a strong interference, and thus the receivers are less sensitive to the desired signals.

Aside from interference, loss is another big issue when it comes to RF front-ends. It is

well known that the resistive loss of a passive component determines its noise figure [10]. The more the Ohmic loss, the more the signal-to-noise ratio (SNR) degradation. This SNR degradation is impossible to recover even if a power amplifier is cascaded to boost up the signal power. Therefore, Ohmic loss of passive components is always a critical criterion in their design.

Time-varying transmission lines are transmission lines whose characteristic impedances are modulated in time by an electromagnetic wave [1–4, 11]. It was introduced as a unique type of transmission line structure that offers non-reciprocity through its uni-directional frequency translation without using magnetic material [1–4]. TVTL is of great interest to people in that: 1) it can offer a decent amount of gain either at original signal band or at converted signal bands; 2) it introduces less amount of noise to the system; 3) it supports full-duplex system, i.e. simultaneous transmit and receive; and 4) it is compatible with integrated circuits.

1.2 Previous Work: Time-varying Transmission Lines (TVTL) as Circulator

Circulator is a non-reciprocal device, in which a signal entering any port is transmitted to the next port in rotation only. For example, signal entering port 1 can only be directed to port 2, while signal entering port 2 can only be transmitted to port 3, and so on in a similar fashion (See Figure 1.1a). Figure 1.1b shows a simultaneous transmit and receive (STAR) front-end enabled by a circulator, where an antenna is attached to port 1, a receiver is attached to port 2, and a transmitter is attached to port 3. This STAR transceiver functions as follows. When a receiving electromagnetic wave is captured by the antenna, it can only be directed to the receiver at port 2. On the other hand, the information sent out by the transmitter can only be routed to port 1 and radiated by the antenna. The circulator prevents transmitted signals from entering the receiver in the same transceiver, and vice versa.

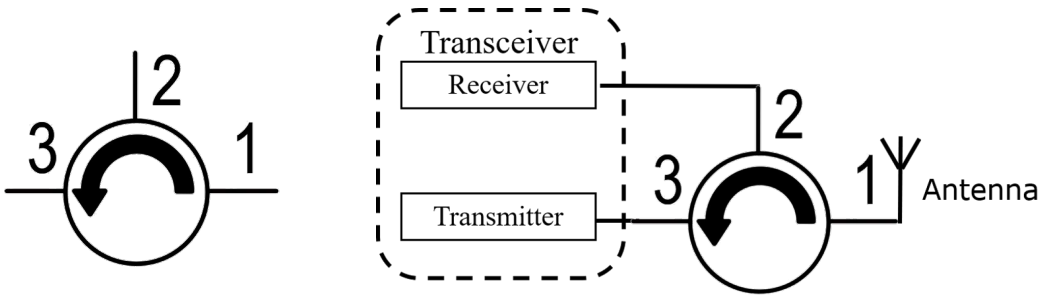

(a) (b)

Figure 1.1: (a) Example: circulator with counterclockwise circulation; (b) Simultaneous transmit and receive (STAR) system enabled by TVTL.

Time-varying transmission lines (TVTL) has uni-directional frequency translation property [1–4], which may be utilized as a circulator. The concept of TVTL as a circulator [1] is illustrated in Figure 1.2.

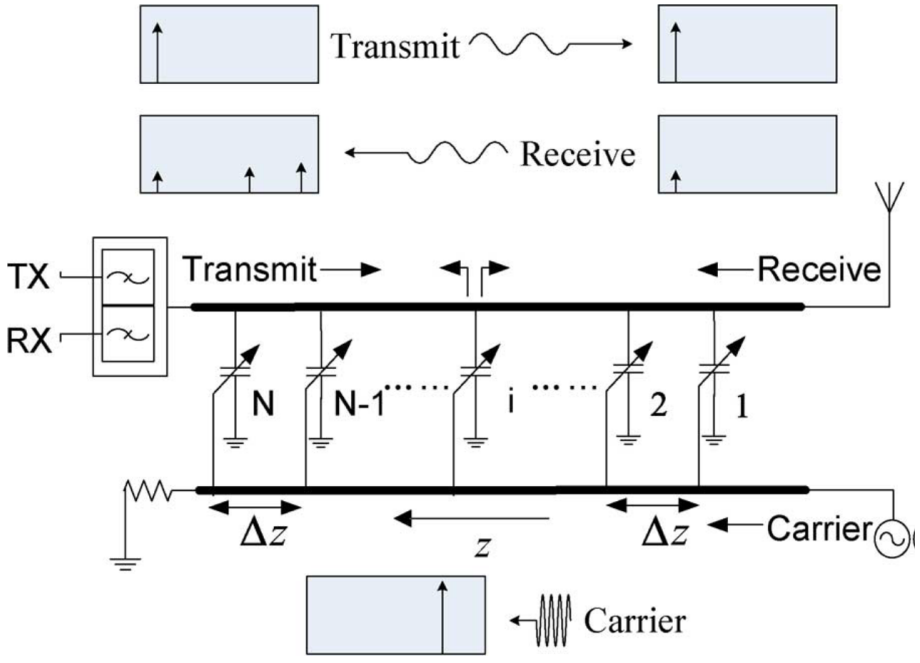

Figure 1.2: Concept of TVTL as a circulator [1].

When a received signal travels in the same direction as the carrier wave, i.e. from right

to left in this case, it will be mixed with the carrier signal. Harmonics and intermodulation terms will then be generated at the transceiver port. The transmitted signal, however, travels in the opposite direction to that of the carrier wave, i.e. from left to right in this case. It remains unaffected by TVTL when it arrives at the antenna port. A diplexer is applied at the transceiver port, i.e. left-hand side in this case, to separate the received and transmitted signals at different frequencies in the transceiver. The operating frequency of the received signal and transmitted signal at antenna port can be the same simultaneously without intereferencing each other, and therefore, achieving simultaneous transmit and receive.

As reported in [2], the circulator achieved with a single MMIC TVTL can achieve a small amount of conversion gain while offering more than 10 dB of isolation for frequency from 1 GHz to 1.5 GHz. The circulator with balanced structure has slightly smaller gain, however, it can achieve 15 more dB of isolation. These are illustrated in Figure 1.3 and Figure 1.4.

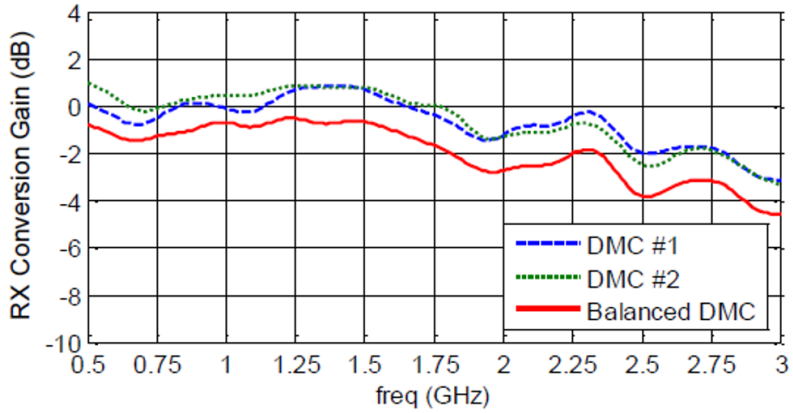

Figure 1.3: Measured conversion gain/loss of the receiving path [2].

1.3 Outline of the Thesis

In this thesis, the parametric amplification modes and noise performance of time-varying transmission lines (TVTL) were analyzed in Chapter 2. In order to observe the parametric amplification behavior predicted by the theory, ideal and monolithic integrated TVTLs were designed and simulated in Chapter 3. In Chapter 4, experiments were performed on several

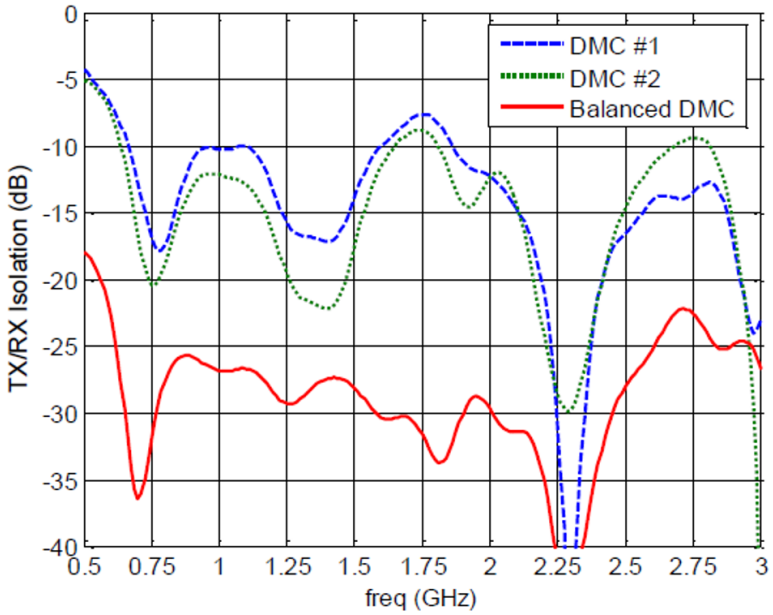

Figure 1.4: Measured isolation between transmitting and receiving paths [2].

fabricated MMIC TVTLs. It is observed in real circuits that both parametric amplification modes exist. These modes can be utilized in frequency translational RF receiver to tackle adjacent channel interference, and they can also be applied in designing novel RF components with lower loss and lower noise.

CHAPTER 2

Theory and Analysis of Time-varying Transmission Lines (TVTL)

Time-varying transmssion lines are the transmission lines whose dielectric properties vary as a function of time and space. They were first proposed by Professor Tien [11] in 1958 with time-varying inductance, and they were intensively studied in the following two decades due to their major applications in traveling wave parametric amplifiers [3, 12]. In recent years, TVTLs with time-varying capacitance have been proposed as one of the most promising structures that offer non-reciprocal frequency translation without using magnetic materials [1]. Its sinusoidal parametric amplification with almost no additional noise is widely discussed and applied in building RF components [2]. Exponential parametric amplification is another parametric amplification mode in TVTLs. It is achieved when the upper sideband ω_{m+s} of the converted signals falls into the stopband of TVTLs. In this chapter, the fundamental concepts of time-varying transmission lines (TVTL) will first be reviewed. In the following section, the mathematical derivations of the two parametric amplification modes in TVTLs will be discussed. The noise figure analysis of TVTLs will be shown in Section 2.3.

2.1 Fundamentals of Time-varying Transmission Lines (TVTL)

Figure 2.1 shows the lumped-element circuit model for a classic lossless transmission line. A time-varying transmission line is formed when its reactance, either capacitance or inductance,

changes with time and space. The unit cells of three types of TVTL are illustrated in Figure 2.2.

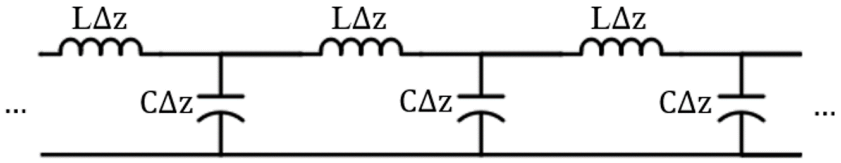

Figure 2.1: Lumped-element circuit model for a classic lossless transmission line.

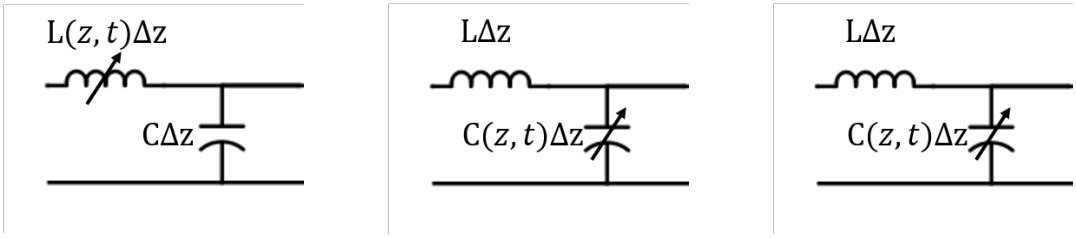

(a) (b) (c)

Figure 2.2: Lumped-element circuit models for different classes of time-varying transmission line (TVTL). (a) TVTL with variable inductance. (b) TVTL with variable capacitance. (c) TVTL with variable inductance and capacitance.

Since variable capacitors are much easier to implement in real circuits, TVTLs with time-varying capacitance are of major interests in the society. They will be the main focus of this thesis, and the following discussions and derivations are based on this type of TVTL. Moreover, continuous TVTL is dispersion-free, however, shock waves may form before anything interesting can happen [13]. Discrete implementations or periodic structures are preferred to create bandgaps and cutoff frequencies to suppress the undesired shock waves. A discrete TVTL with time-varying capacitance is usually approached by periodically loading a classic transmission line with equally-spaced varactor diodes [1], as illustrated in Figure 2.3. The voltages across these varactor diodes are modulated by a carrier wave traveling along the transmission line, resulting in distributed variable capacitors in time and space.

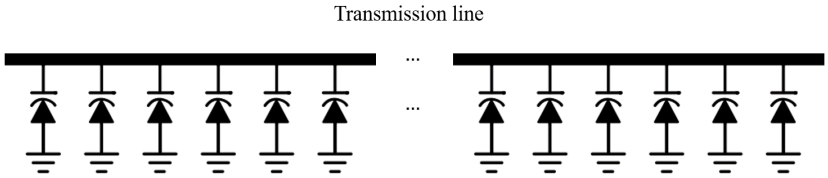

Figure 2.3: Practical implementation of TVTL: a transmission line periodically loaded with varactor diodes.

2.2 Parametric Amplification in Time-varying Transmission Lines (TVTL)

The parametric amplification theory of TVTL has been well-studied in literature [1, 11, 14]. The formulation of the thoery are carefully reviewed in this section as the thoretical reference of the following circuit design. Refer to Figure 2.4 for the lumped-element circuit model of transmission line with time-varying capacitance.

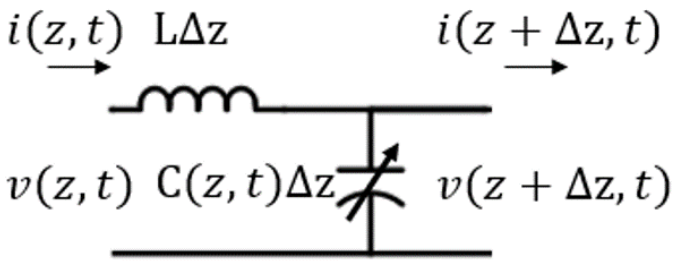

Figure 2.4: Lumped-elecment circuit model of TVTL with variable capacitance; voltages and currents are defined for both ports.

Define voltage and current at the left-hand side as $v(z,t)$ and $i(z,t)$, and voltage and current at the right-hand side as $v(z+\Delta z,t)$ and $i(z+\Delta z,t)$ respectively. Then, Kirchhoff's

voltage law and Kirchhoff's current law can be applied to give:

$$v(z,t) - L\Delta z\frac{\partial i(z,t)}{\partial t} - v(z+\Delta z,t) = 0 \tag{2.1a}$$

$$i(z,t) - \Delta z\frac{\partial\left[C(z,t)v(z+\Delta z,t)\right]}{\partial t} - i(z+\Delta z,t) = 0 \tag{2.1b}$$

Divide equation (2.1a) and (2.1b) by Δz and let $\Delta z \to 0$. The resulting telegrapher's equations for TVTL can be written as:

$$\frac{\partial v(z,t)}{\partial z} = -L\frac{\partial i(z,t)}{\partial t} \tag{2.2a}$$

$$\frac{\partial i(z,t)}{\partial z} = -\frac{\partial\left[C(z,t)v(z,t)\right]}{\partial t} \tag{2.2b}$$

Combine equation (2.2a) and (2.2b) and eliminate $i(z,t)$ at both sides, one can derive the following wave equation:

$$\frac{\partial^2 v(z,t)}{\partial z^2} = L\frac{\partial^2\left[C(z,t)v(z,t)\right]}{\partial t^2} \tag{2.3}$$

Now, let's assume the capacitance of the transmission line is modulated by a traveling wave at frequency ω_m, and the value of capacitance can be written in the following form:

$$C(z,t) = C_0 + C_m\cos(\omega_m t - \beta_m z + \phi_m) \tag{2.4}$$

where $v_p = \omega_m/\beta_m = 1/\sqrt{LC_0}$ is the phase velocity of the carrier wave.

Equation (2.3) then becomes:

$$\frac{\partial^2 v(z,t)}{\partial z^2} = LC_0\frac{\partial^2 v(z,t)}{\partial t^2} + LC_m\frac{\partial^2\left[\cos(\omega_m t - \beta_m z + \phi_m)v(z,t)\right]}{\partial t^2} \tag{2.5}$$

2.2.1 Sinusoidal Parametric Amplification

When a signal at frequency ω_s is injected into the transmission line, harmonics at frequencies $k\omega_s$ and intermodulation tones at frequencies $i\omega_m \pm k\omega_s$ will be generated due to the last term in equation (2.5) on the right hand side, where $i,\ k$ are integers. Assume the tones at frequencies ω_s, $\omega_{m-s} = \omega_m - \omega_s$, and $\omega_{m+s} = \omega_m + \omega_s$ are the most significant terms among all the tones in TVTL. Thus, one may limit the discussion to these three tones.

Let:

$$v_s(z,t) = V_s(z)\cos(\omega_s t - \beta_s z + \phi_s) \tag{2.6a}$$

$$v_{m-s}(z,t) = V_{m-s}(z)\cos(\omega_{m-s} t - \beta_{m-s} z + \phi_{m-s}) \tag{2.6b}$$

$$v_{m+s}(z,t) = V_{m+s}(z)\cos(\omega_{m+s} t - \beta_{m+s} z + \phi_{m+s}) \tag{2.6c}$$

$$v(z,t) = v_s(z,t) + v_{m-s}(z,t) + v_{m+s}(z,t) \tag{2.6d}$$

and:

$$i_s(z,t) = I_s(z)\cos(\omega_s t - \beta_s z + \phi_s) \tag{2.7a}$$

$$i_{m-s}(z,t) = I_{m-s}(z)\cos(\omega_{m-s} t - \beta_{m-s} z + \phi_{m-s}) \tag{2.7b}$$

$$i_{m+s}(z,t) = I_{m+s}(z)\cos(\omega_{m+s} t - \beta_{m+s} z + \phi_{m+s}) \tag{2.7c}$$

$$i(z,t) = i_s(z,t) + v_{m-s}(z,t) + v_{m+s}(z,t) \tag{2.7d}$$

where $\beta_{m-s} = \beta_m - \beta_s$ and $\beta_{m+s} = \beta_m + \beta_s$ are the propagation constants of signals at frequencies ω_{m-s} and ω_{m+s} respectively.

Substitute equation (2.6) and equation (2.7) into equation (2.2b) and consider the terms

at frequency ω_{m-s} only:

$$\frac{\partial I_{m-s}(z)}{\partial z}\cos(\omega_{m-s}t-\beta_{m-s}+\phi_{m-s})+I_{m-s}(z)\beta_{m-s}\sin(\omega_{m-s}t-\beta_{m-s}z+\phi_{m-s})$$
$$=C_0\omega_{m-s}V_{m-s}(z)\sin(\omega_{m-s}t-\beta_{m-s}z+\phi_{m-s})+\frac{1}{2}C_m\omega_{m-s}V_s(z)\sin(\omega_{m-s}-\beta_{m-s}z+\phi_m-\phi_s) \tag{2.8}$$

Similarly, if one only consider the terms at frequency ω_{m+s}, then:

$$\frac{\partial I_{m+s}(z)}{\partial z}\cos(\omega_{m+s}t-\beta_{m+s}+\phi_{m+s})+I_{m+s}(z)\beta_{m+s}\sin(\omega_{m+s}t-\beta_{m+s}z+\phi_{m+s})$$
$$=C_0\omega_{m+s}V_{m+s}(z)\sin(\omega_{m+s}t-\beta_{m+s}z+\phi_{m+s})+\frac{1}{2}C_m\omega_{m+s}V_s(z)\sin(\omega_{m+s}-\beta_{m+s}z+\phi_m+\phi_s) \tag{2.9}$$

Let the phase of the carrier to be the reference phase, i.e. $\phi_m = 0$, without losing generality. Furthermore, apply initial conditions: $V_s(0) = V_0$, $V_{m-s}(z) = V_{m+s}(z) = 0$, and $I_{m-s}(z) = I_{m+s}(z) = 0$ in equation (2.8) and equation (2.9). One can lead to the following phase conditions:

$$\cos(\phi_{m-s}+\phi_s)=0 \tag{2.10}$$

and:

$$\cos(\phi_{m+s}-\phi_s)=0 \tag{2.11}$$

Next, substitute equation (2.6) into equation (2.5), and incorporate the phase conditions in equation (2.10) and equation (2.11). Equation (2.5) can be simplified into the following forms:

$$\frac{\partial V_s(z)}{\partial z}+\frac{1}{4}\frac{C_m}{C_0}\beta_s\left[V_{m-s}(z)-V_{m+s}(z)\right]=0 \tag{2.12a}$$
$$\frac{\partial V_{m-s}(z)}{\partial z}+\frac{1}{4}\frac{C_m}{C_0}\beta_{m-s}V_s(z)=0 \tag{2.12b}$$
$$\frac{\partial V_{m+s}(z)}{\partial z}+\frac{1}{4}\frac{C_m}{C_0}\beta_{m+s}V_s(z)=0 \tag{2.12c}$$

Define $\xi = C_m/C_0$ as the modulation index. Then, the solutions of equation (2.12) can be derived as follows:

$$V_s(z) = V_0 \cos(\frac{1}{2\sqrt{2}}\xi\beta_s z) \tag{2.13a}$$

$$V_{m-s}(z) = -\frac{V_0}{\sqrt{2}}\frac{\beta_{m-s}}{\beta_s}\sin(\frac{1}{2\sqrt{2}}\xi\beta_s z) \tag{2.13b}$$

$$V_{m+s}(z) = -\frac{V_0}{\sqrt{2}}\frac{\beta_{m+s}}{\beta_s}\sin(\frac{1}{2\sqrt{2}}\xi\beta_s z) \tag{2.13c}$$

which represent the sinusoidal parametric amplification mode in TVTL.

From equation (2.13b) and (2.13c), it is possible to get substantial amount of gain from TVTL as long as the separation between orignal frequency, ω_s, and converted frequencies, ω_{m-s} or ω_{m+s} is much larger than 1. This has been observed in [2], where a more than 0 dB conversion gain is obtained at frequencies ranging from 1 GHz to 1.5 GHz. Similar simulation and measurement results will be shown in Chapter 3 and Chapter 4 as well.

2.2.2 Exponential Parametric Amplification

Exponential parametric amplification is another parametric amplification mode in TVTL. It is formed when the converted signal at frequency ω_{m+s} is short-circuited at the output, i.e. $V_{m+s} = 0$. Expoential parametric amplification can be achieved by carefully designing the cutoff frequency of the discrete TVTL, as shown in Figure 2.3, to suppress the upper sideband ω_{m+s} of the converted signals. The voltages in TVTL under exponential amplification mode becomes:

$$v_s(z,t) = V_s(z)\cos(\omega_s t - \beta_s z + \phi_s) \tag{2.14a}$$

$$v_{m-s}(z,t) = V_{m-s}(z)\cos(\omega_{m-s} t - \beta_{m-s} z + \phi_{m-s}) \tag{2.14b}$$

$$v_{m+s}(z,t) = 0 \tag{2.14c}$$

$$v(z,t) = v_s(z,t) + v_{m-s}(z,t) \tag{2.14d}$$

The relationship between the voltages at frequency ω_s and ω_{m-s} can thus be written as:

$$\frac{\partial V_s(z)}{\partial z} + \frac{1}{4}\xi\beta_s V_{m-s}(z) = 0 \tag{2.15a}$$

$$\frac{\partial V_{m-s}(z)}{\partial z} + \frac{1}{4}\xi\beta_{m-s} V_s(z) = 0 \tag{2.15b}$$

The solutions to equation (2.15) are:

$$V_s(z) = V_0 \cosh(\frac{1}{4}\xi\sqrt{\beta_s\beta_{m-s}}z) \tag{2.16a}$$

$$V_{m-s}(z) = -V_0\sqrt{\frac{\beta_{m-s}}{\beta_s}}\sinh(\frac{1}{4}\xi\sqrt{\beta_s\beta_{m-s}}z) \tag{2.16b}$$

which indicate exponential parametric amplification at both frequency ω_s and ω_{m-s}. Moreover, the exponential parametric effect should be more prominant at lower sideband ω_{m-s} when transmission line is short because $\cosh(x)$ is much larger than that of $\sinh(x)$ when $x \approx 0$. In Chapter 4, measurement results of monolithic integrated TVTLs will be shown to provide proofs of the theory.

2.3 Noise Performance of Time-varying Transmission Lines (TVTL)

Ideally, time-varying transmission lines should introduce zero noise because there are not any lossy components in neither transmission lines nor varactor diodes. In reality, however, transmission lines and varactor diodes are evitably lossy due to finite conductivity of metal layers. This passive loss will introduce noise to the system.

The noise figure of TVTLs is well analyzed in [1], and it will be revisited here for completeness. To simplify the analysis of noise figure, one may consider the loss of transmission line as the loss of varactor diodes. Therefore, thermal noise comes from varactor diodes only. Due to the frequency conversion property of TVTL, there exist two noise sources that

contribute to noise power at converted frequency bands of TVTL. The first source generates thermal noise at the original frequency ω_s. This noise power is then converted to frequencies $\omega_{m\pm s}$ at the output of TVTL. Aside from that, resistive loss of varactor diodes also generate thermal noise directly at frequencies $\omega_{m\pm s}$. This results in the other portion of noise power at the output of TVTL.

In the analysis, let us assume TVTL is under thermal equilibrium condition, i.e. the total noise power at the output of TVTL equals to that generated by the noise resistor at the input, that is:

$$N_0 = kT_0B = G_skT_0B + G_sN_s \tag{2.17}$$

where T_0 is the temperature of the network, $G_s = \exp(-2\alpha_s z)$ is the power gain of TVTL at frequency ω_s, and α_s is the attenuation constant of TVTL at frequency ω_s.

The noise added by TVTL at frequency ω_s is thus:

$$N_s = kT_0B(e^{2\alpha_s z} - 1) \tag{2.18}$$

Now, let us consider a discrete implementation of TVTL with finite number of varactor diodes. Denote N as the number of varactor diodes which are equally-spaced along the transmission line. Then, the noise power generated by TVTL can also be represented by the summation of thermal noise from each varactor diode. Assume the thermal noise introduced by each varactor diode has the same statistics. The noise added by TVTL at frequency ω_s can be written as:

$$N_s = \frac{1}{Z_B}\sum_{i=1}^{N} v_{ni}^2 = \frac{N}{Z_B}v_n^2 \tag{2.19}$$

where v_{ni} is the noise voltage across the $i-$th varactor diodes and Z_B is the Bloch impedance of TVTL. Noted that the noise voltages have the same rms value v_n because they have the same statistics.

When noise at original frequency ω_s is generated by varactor diodes, it will be converted to frequencies $\omega_{m\pm s}$ after passing TVTL. One may consider each varactor diode as a capacitive

mixer whose conversion gain at frequencies $\omega_{m\pm s}$ are [1]:

$$g_{c,m\pm s} = \frac{1}{4}(\omega_m \pm \omega_s) Z_B C_m \tag{2.20}$$

Once thermal noise is generated by the $i-$th varactor diode in TVTL, it will be converted to frequencies $\omega_{m\pm s}$ by the following $(N-i)$ varactor diodes with conversion gain $g_{c,m\pm s}$ in equation (2.20). The converted noise power at frequencies $\omega_{m\pm s}$ at the output is thus given as:

$$\begin{aligned} N_{1,m\pm s} &= \frac{g_{c,m\pm s}^2}{Z_B} \sum_{i=1}^{N} (N-i+1)^2 v_{ni}^2 \\ &= \frac{N(N+1)(2N+1)}{6Z_B} g_{c,m\pm s}^2 v_n^2 \\ &\approx \frac{N^3 g_{c,m\pm s}^2 v_n^2}{3Z_B} \\ &= \frac{N^2 g_{c,m\pm s}^2}{3} N_s \end{aligned} \tag{2.21}$$

The other portion of noise power at the output of TVTL is the result of thermal noise directly emitted at $\omega_{m\pm s}$ by varactor diodes. This can be expressed as:

$$N_{2,m\pm s} = kT_0 B(e^{2\alpha_{m\pm s} z} - 1) \tag{2.22}$$

where $\alpha_{m\pm s}$ are the attenuation constants of transmission lines periodically loaded with varactor diodes at frequencies $\omega_{m\pm s}$.

The noise figure of TVTL is thus expressed as:

$$\begin{aligned} F_{m\pm s} = \frac{SNR_i}{SNR_o} &= \frac{S_i}{S_o}\frac{N_o}{N_i} \\ &= \frac{N^2 g_{c,m\pm s}^2 kT_0 B + N_{1,m\pm s} + N_{2,m\pm s}}{N^2 g_{c,m\pm s}^2 kT_0 B} \\ &= 1 + \frac{1}{3}(e^{2\alpha_s z} - 1) + \frac{e^{2\alpha_{m\pm s} z} - 1}{N^2 g_{c,m\pm s}^2} \end{aligned} \tag{2.23}$$

When loss is small, i.e. $\alpha_s \approx 0$ and $\alpha_{m\pm s} \approx 0$, one may apply the following approxiamtions:

$$e^{2\alpha_s z} - 1 \approx 2\alpha_s z = \frac{\beta_s z}{Q_s} \tag{2.24a}$$

$$e^{2\alpha_{m\pm s} z} - 1 \approx 2\alpha_{m\pm s} z = \frac{\beta_{m\pm s} z}{Q_{m\pm s}} \tag{2.24b}$$

where Q_s and $Q_{m\pm s}$ are the quality factors of TVTL at three different frequencies respectively. They can be estimated based on the quality factors of varactor diodes at corresponding frequencies, $Q_{d,s}$ and $Q_{d,m\pm s}$, and the capacitance of the unloaded transmission line C_{TRL} as:

$$Q_s \approx (1 + \frac{C_{TRL}}{C_m}) Q_{d,s} \tag{2.25a}$$

$$Q_{m\pm s} \approx (1 + \frac{C_{TRL}}{C_m}) Q_{d,m\pm s} \tag{2.25b}$$

Furthermore, when $\frac{1}{2\sqrt{2}}\xi\beta_s z \ll \frac{\pi}{2}$, i.e. length of TVTL is short enough, equation (2.13b) and equation(2.13c) may be approximated by:

$$\begin{aligned} \left|\frac{V_{m\pm s}(z)}{V_0}\right| &= \frac{1}{\sqrt{2}}\frac{\beta_{m\pm s}}{\beta_s}\sin(\frac{1}{2\sqrt{2}}\xi\beta_s z) \\ &\approx \frac{1}{\sqrt{2}}\frac{\beta_{m\pm s}}{\beta_s} \cdot \frac{1}{2\sqrt{2}}\xi\beta_s z \\ &= \frac{1}{4}\xi\beta_{m\pm s} z \end{aligned} \tag{2.26}$$

These lead to:

$$N^2 g_{c,m\pm s}^2 = \left(\frac{1}{4}\xi\beta_{m\pm s} z\right)^2 \tag{2.27}$$

Therefore, the noise figure in equation (2.23) can be simplified into:

$$NF(dB) = 10\log_{10}(1 + \frac{1}{3}\frac{\beta_s z}{Q_s} + \frac{16}{\xi^2}\frac{1}{Q_{m\pm s}\beta_{m\pm s} z}) \tag{2.28}$$

It can be seen from equation (2.28) that the noise generated by varactor diodes directly at $\omega_{m\pm s}$ contributes the most to the noise figure of TVTL when transmission line is short. Moreover, the quality factors and modulation index of varactor diodes play an important role in reducing noise power generated by TVTL. The higher the quality factors, and the higher the modulation index, the lower the noise figure.

CHAPTER 3

Design and Simulation of Time-varying Transmission Lines (TVTL)

In the previous chapter, the fundamental concept of time-varying transmission lines (TVTL) was first reviewed in Section 2.1. The mathematical representations of two parametric amplification modes were then disscussed in Section 2.2. Last but not least, the noise performance of TVTL was analyzed in Section 2.3. Now that one has understood the theory of TVTL, it is time to observe the behavior of parametric amplification in both ideal TVTL and real circuits, such as monolithic microwave integrated circuit (MMIC). In this chapter, the design of ideal TVTL will fisrt be introduced, and the simulated parametric amplification will also be shown in Section 3.1. In Section 3.2, the design of MMIC TVTL will be discussed.

3.1 Ideal Time-varying Transmission Lines (TVTL)

3.1.1 Design of Ideal Time-varying transmission lines (TVTL)

In this research, ideal TVTL was designed and simulated in Advanced Design System (ADS), a commerical software. The ideal TVTL is designed based on Figure 2.3 except that the varactor diodes were replaced by capacitors whose capacitance values varied linearly with the applied voltages. The unit cell of the TVTL is depicted in Figure 3.1a. The voltage-dependent capacitors were to simulate the capacitance variations of varactor diodes under different applied voltages, as shown in Figure 3.1b. The resistor in series with the voltage-

dependent capacitor was to represent the loss in TVTL.

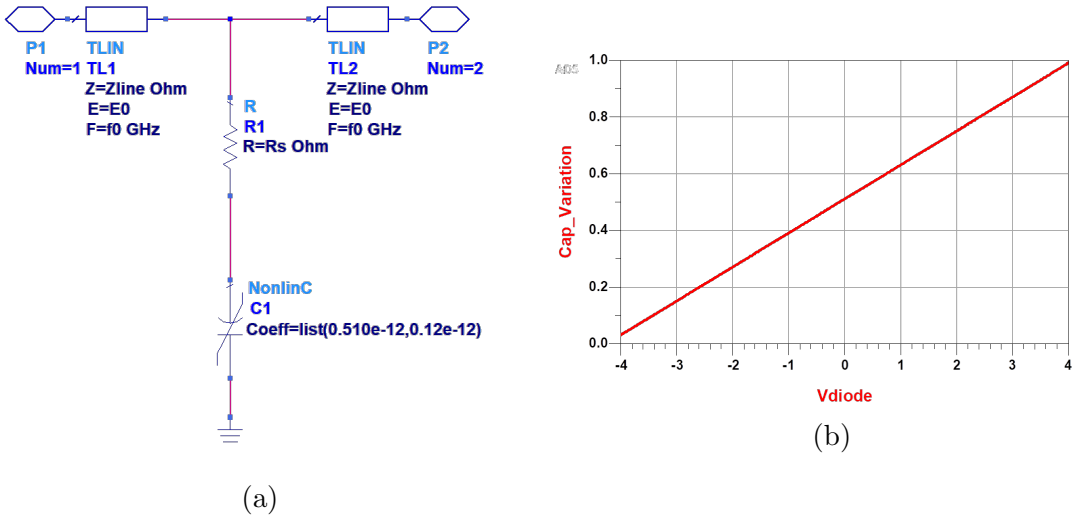

(a) (b)

Figure 3.1: Schematic of ideal TVTL: (a) Unit cell; (b) Capacitance variation of the voltage-dependent capacitors.

3.1.2 Simulation of Ideal Time-varying Transmission Lines (TVTL)

The curoff frequency of TVTL can be tuned by varying the capacitance value and the length of transmission line in each unit. As shown by the insertion loss in Figure 3.2, the cutoff frequency of the designed 12-unit TVTL is 6.7 GHz. In addition, the return loss in Figure 3.2 indicates that the 12-unit TVTL is well matched to 50 ohm up to 5 GHz.

The conversion gain of the ideal TVTL is simulated with ADS Harmonic Balance (HB) simulation. Signals whose frequencies ranging from 0.5 GHz to 1.5 GHz were selected to be the input signals. Furthermore, the frequecy of the pumping carrier was chosen to be 5 GHz in order to observe the sinusoidal parametric amplification. Under such conditions, both upper sideband ω_{m+s} and the lower sideband ω_{m-s} of the converted signals are within the passband of the ideal TVTL. The power of the input signals and the carrier pump were -10 dBm and 20 dBm respectively. As shown in Figure 3.3, more than 1 dB of conversion gain can be obtained for both upper sideband ω_{m+s} and lower sideband ω_{m-s} of the converted signals for all input frequencies. The maximum conversion gain is 5.6 dB for upper sideband

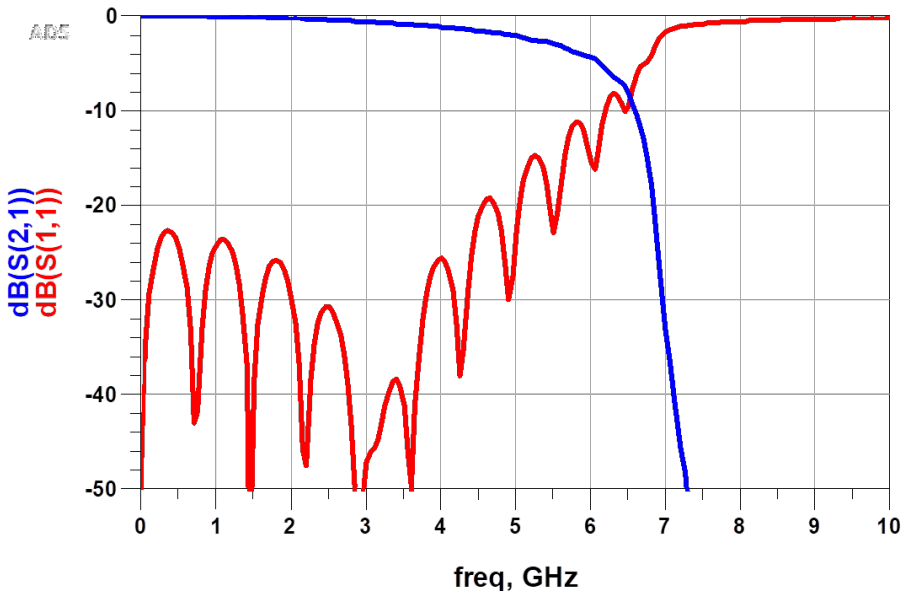

Figure 3.2: Simulated S-parameter of ideal TVTL; blue: insertion loss of TVTL; red: return loss of TVTL.

and 6.4 dB for lower sideband. Moreover, the conversion gain for the lower sideband is higher than that of the upper sideband when frequency is smaller than 1.25 GHz. This is mainly due to the higher insertion loss at higer frequencies. Therefore, the ratio β_{m+s}/β_s in equation (2.13c) must be large enough in order to compensate for the insertion loss of TVTL and get higher conversion gain.

To observed exponential parametric amplification, a 20 dBm 6.0 GHz signal was pumped into TVTL as the carrier, and -10 dBm 0.1 GHz to 1.1 GHz signals were selected as the input signals. Then, upper sideband ω_{m+s} of some converted signals will fall into the stopband of the TVTL, resulting in a two-tone parametric coupling mode that offers exponential amplification at ω_s. It can be seen from Figure 3.4 that the power gain suddenly increases at frequency around 0.4 GHz, which indicating a transition between sinusoidal parametric amplification mode and exponential parametric amplification mode.

Furthermore, when sweeping the carrier frequencies from 6.1 GHz to 6.3 GHz with a 0.2 GHz step, the starting point of exponential amplification shifts with carrier frequency correspondingly as shown in Figure 3.5.

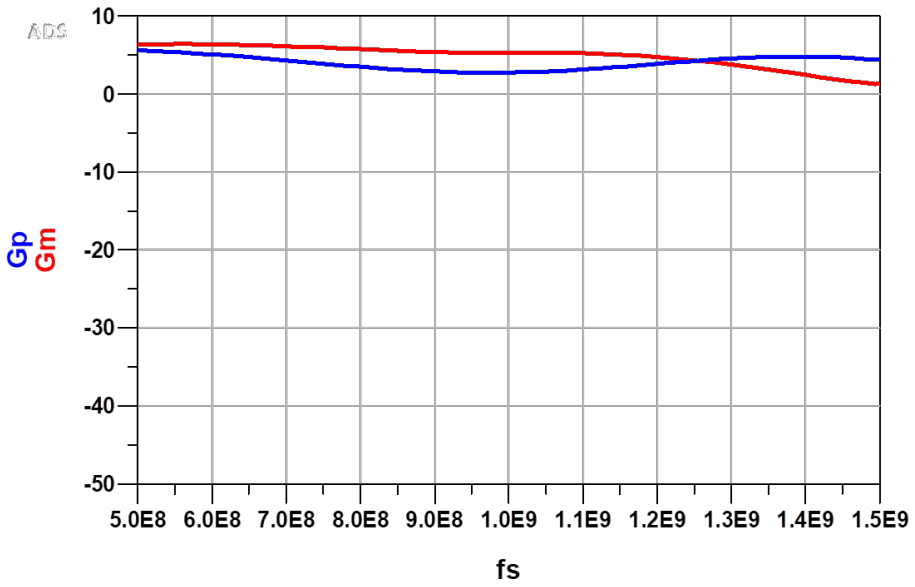

Figure 3.3: Simulated conversion gain of ideal TVTL; blue: upper sideband ω_{m+s}; red: lower sideband ω_{m-s}.

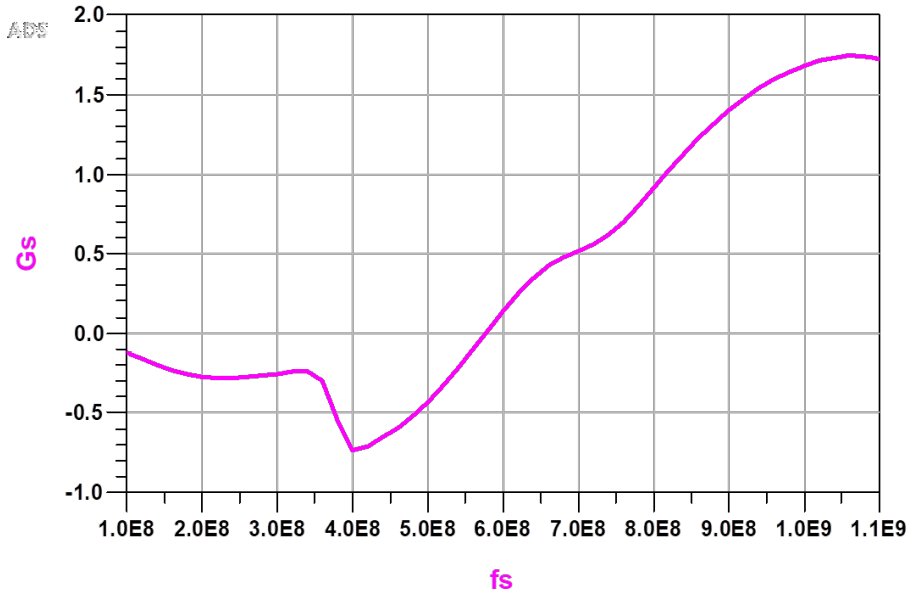

Figure 3.4: Simulated exponential amplification effect at ω_s with fc = 6.0 GHz.

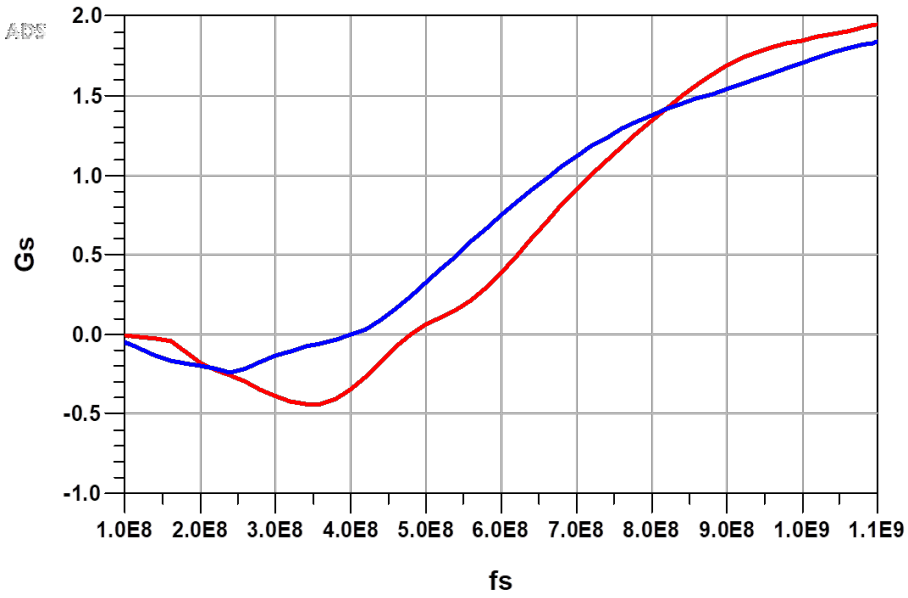

Figure 3.5: Simulated exponential amplification effect at ω_s with frequency sweeping from 6.1 GHz to 6.3 GHz.

3.2 Time-varying Transmission Lines(TVTL) with Monolithic Microwave Integrated Circuit (MMIC)

So far, we have observed the parametric amplification behavior in ideal time-varying transmission lines (TVTL), so the next step is to verify it in real circuits. In this research, TVTLs are implemented with monolithic microwave integrated circuit (MMIC) technology because MMIC devices usually have superior performance at microwave frequencies. Besides, chip-scale design can reduce circuit area, parasitics, and undesired package uncertainty with the help of commerical computer-aided design (CAD) tools. Last but not least, on-chip integration is required for massive production in RF front-ends of wireless communication systems such as mobile phones, wifi modem, and etc.

Varactor diodes are the key to TVTL design because they originate the time-varying electromagnetic behavior of TVTL. High performance varactor diodes should offer a wide range of capacitance variations so that TVTL can achieve broadband parametric amplification. They should also be of high quality factors so that they introduce minimum amount of noise

to the system . It is critical to have accurate device model of varactor diode before designing TVTL. Therefore, measurement-based varactor diodes modeling will first be discussed in Section 3.2.1. Then, the design of MMIC TVTL based on thoery discussed in Section 2.2 and model derived in Section 3.2.1 will be reviewed in Section 3.2.2.

3.2.1 Varactor Diode Modeling

Device modeling has always been an important part in IC design because good device models enable engineers to better understand and predict the behavior of the designed circuits. In TVTL design, it is important to have accurate varactor diode models because performance of TVTL greatly depends on the quality of varactor diodes. In this research, measurement-based varactor diode modeling method is applied, and the procedure of this method is shown in Figure 3.6.

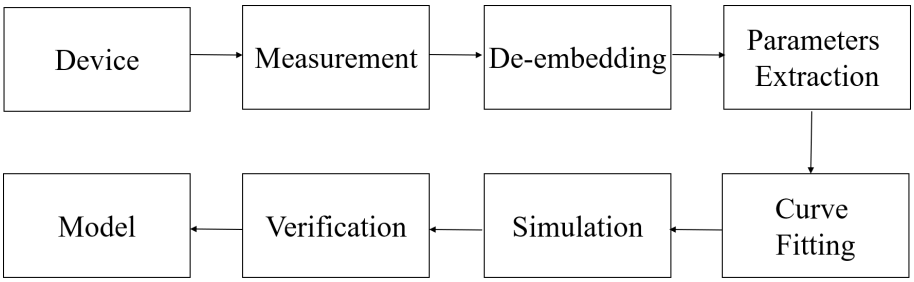

Figure 3.6: Block diagram of measurement-based varactor diode modeling.

During device modeling, the S-parameters of varactor diodes of different dimensions were first measured using a vector network analyzer. Then, the additional phase shifts, which was due to test fixtures including pads and feedlines, were removed from the measurement using through-only de-embedding method as discussed in [15] (See Figure 3.7 for the concept of de-embedding). Through-only de-embedding method was chosen because it only requires one dummy pattern, but yields accurate de-embedding results up to 110 GHz.

Once the S-parameters of the devices themselves were obtained, equivalent circuit parameters were extracted using a Π network as depicted in Figure 3.8. When a varactor diode

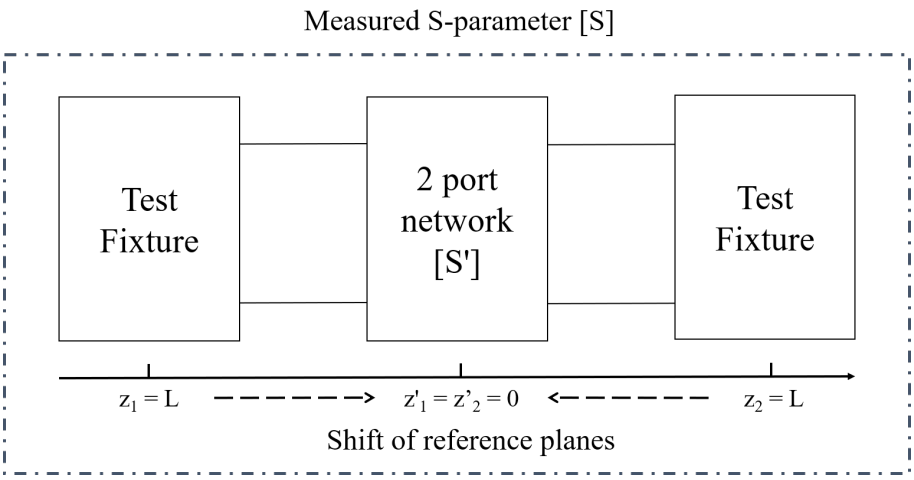

Figure 3.7: Concept of de-embedding; the dashed arrows represent the shift of reference planes

is biased with negative voltages, it behaves like a voltage-voltage dependent capacitor, as represented by the series capacitor C_s in the model. This voltage-dependent capacitor is the most important parameter of varactor diode that needs to be characterized. Figure 3.9 depicts the capacitance variations in terms of biasing voltage. The seris resistor R_s represents the Ohmic loss of a varactor diode, and it plays an important role in determining a varactor diode's quality factor. When a varactor diode is forward biased, it resembles the behavior of a diode, as represented by D_p in parallel with the RC. The current-voltage relationship is shown in Figure 3.10. The two shunt capacitors, C_{p1} and C_{p2} in Figure 3.8, are the parasitic capacitors resulted from gate and drain pads of a varactor diode.

Next, curve fitting was performed on one set of device data, and a functional relationship between the capacitance value and the reversed biasing voltage (C-V) was derived. The equation was then defined as a symbolically-defined device (SDD) in ADS to simulate the C-V behavior of a varactor diode. Lastly, the performance of the model was verified by scaling the the size of the varactor diode in the model and compared the simulation with the corresponding measured result. This is indicated in Figure 3.11, where the blue line is the measured C-V of varactor diode with dimension $5 \times 10 \times 50$, and the red line is the simulated C-V curve based on varactor model extracted from varactor diode with dimension

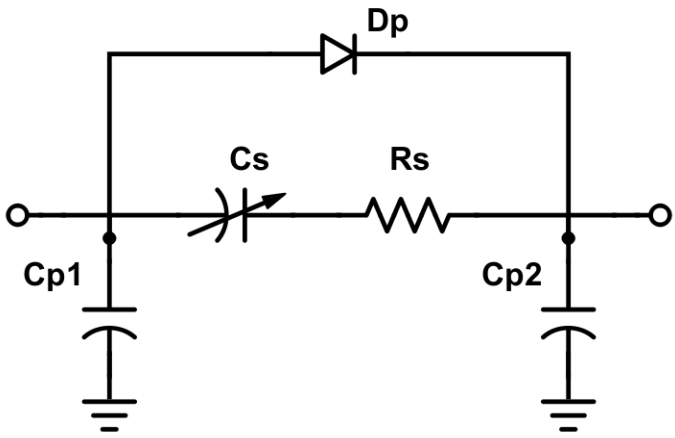

Figure 3.8: Equivalent circuit of varactor diode: Π equivalent.

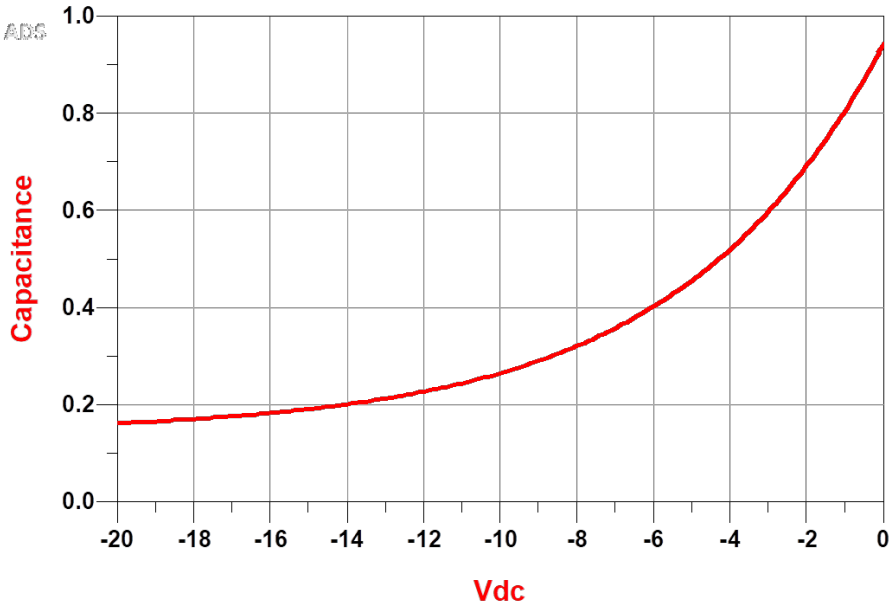

Figure 3.9: Varactor diode C-V behavior: varactor diodes behave as a voltage-dependent capacitor when reversed bias.

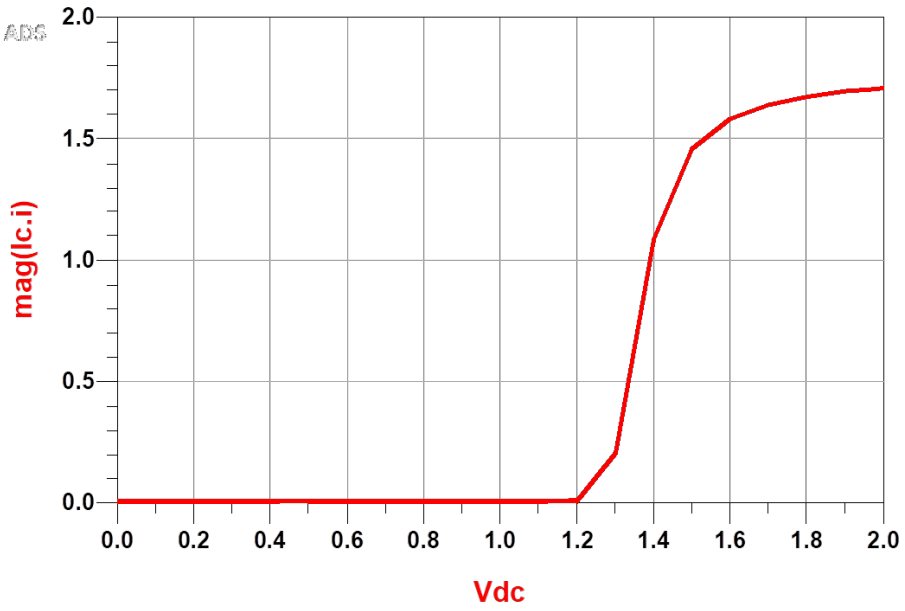

Figure 3.10: Varactor diode I-V behavior when forward biased.

$3 \times 10 \times 50$. The simulated C-V behavior agrees with measured result well.

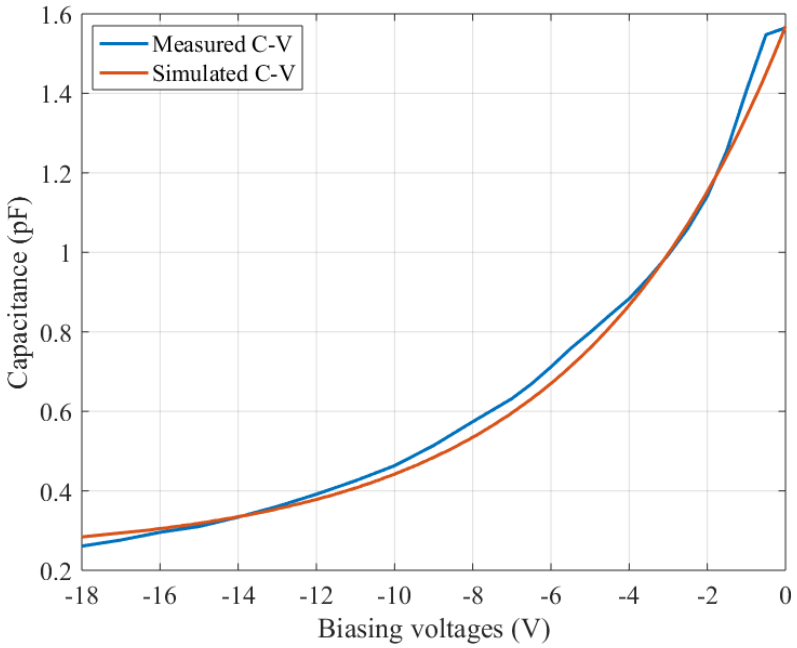

Figure 3.11: Verification of varactor diode model; blue: measured results of varactor diode with dimension $5 \times 10 \times 50$; red: Scaled version of varactor diode model extracted from varactor diode with dimension $3 \times 10 \times 50$.

In addition, the model was also put into TVTL to check its performance by comparing simulation and measurement in a bigger circuit structure. As is shown in Figure 3.12, the simulated insertion loss (red) matches well with the measured insertion loss (blue) of an 8-unit TVTL up to 6.5 GHz. The varactor diode model can help to better predict the small-signal behavior of TVTL.

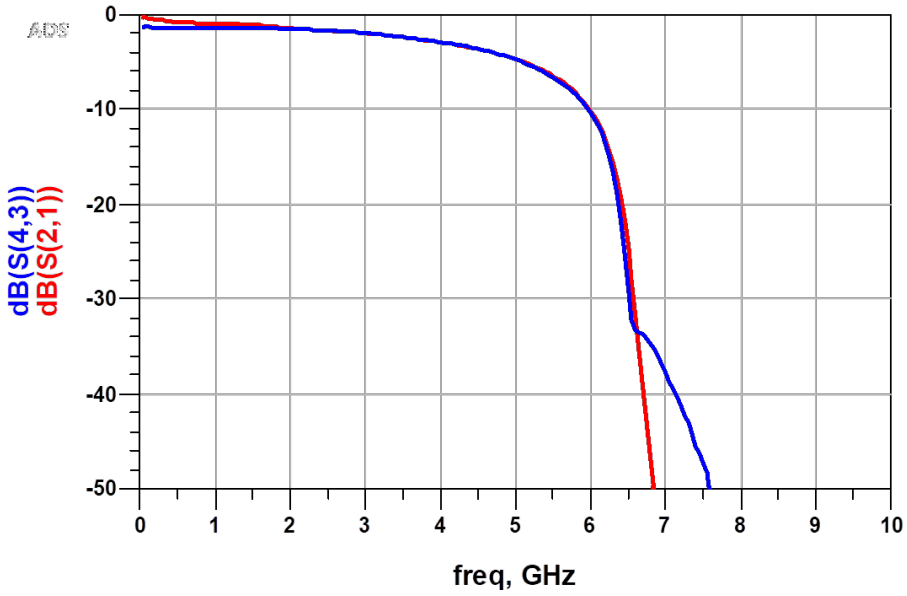

Figure 3.12: Verification of varactor diode model in TVTL; blue: measured insertion loss of an 8-unit TVTL; red: simulated insertion loss of an 8-unit TVTL.

3.2.2 MMIC Time-varying Transmission Lines (TVTL)

Now that we have obtained an accurate measurement-based varactor diode model for design of TVTL, it is time to verify the parametric amplification effects in monolithic microwave integrated circuits (MMIC). The TVTL design is based on the diagram shown in Figure 3.13, where a 63 Ω transmission line is periodically loaded with 16 varactor diodes. The character impedance of the transmission line was chosen to be 63 Ω so that the periodic structure was matched to 50 Ω. Besides, the transmission line was meandered to reduce the chip size. An additional inductor was added in series with varactor diode to reduce the carrier power and boost up conversion gain. The inductance value was small enough, so it would not affect the

impedance matching of TVTL at signal frequency ω_s.

The inductor pumping structure was able to reduce carrier power in that the capacitor of

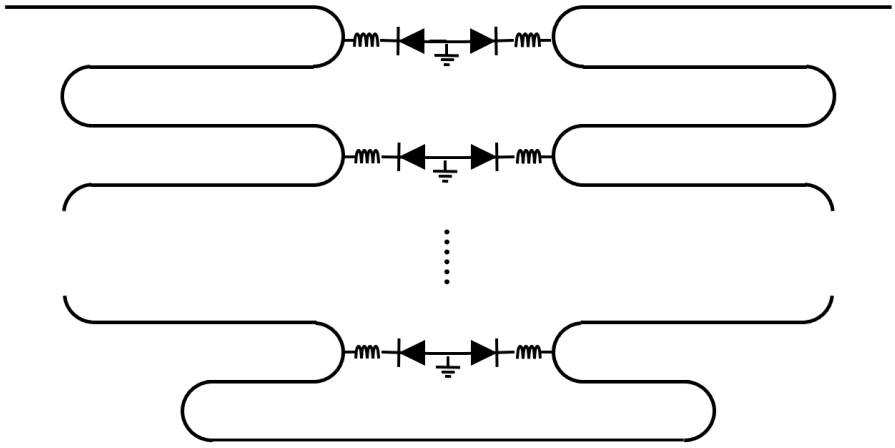

Figure 3.13: Schematic of MMIC TVTL

each varactor diode formed a series LC resonator with the inductor. The voltage across the $i-$th varactor diode v_{di} can be related to the carrier voltage v_{mi} by the following equation:

$$\frac{v_{di}}{v_{mi}} = \frac{1/(j\omega_m C_0)}{j\omega_m L + 1/(j\omega_m C_0)} = \frac{1}{1-\omega_m^2 LC_0} \tag{3.1}$$

When the resonance frequency of the resonantor was designed to be around the carrier frequency ω_m, i.e. $\omega_m^2 LC_0 \approx 1$, the LC resonantor can provide a huge boost to modulation voltage across the varactor diode, and in return, reduce the amount of carrier power comsumed in TVTL.

Moreover, with the help of inductor, it is possible to increase the conversion gain of TVTL because the capacitance modulation index ξ in equation (2.13) and equation (2.16) now becomes:

$$\xi_e = \frac{C_m}{C_0}\frac{1}{1-\omega_m^2 LC_0} = \xi_0 \frac{1}{1-\omega_m^2 LC_0} \tag{3.2}$$

where $\xi_0 = C_m/C_0$ is the capacitance modulation index without inductance pumping.

As show in Figure 3.14, more than 4.5 dB of conversion gain improvement was observed in the lower sideband ω_{m-s} of the converted signal without tunning the pumping inductance

value. Furthermore, a 7.90 dB conversion gain improvement in the lower sideband ω_{m-s} and a 2.87 dB conversion gain improvement in the upper sideband ω_{m+s} of the converted signal was also obtained when optimizing the inductance value as depicted in Figure 3.15.

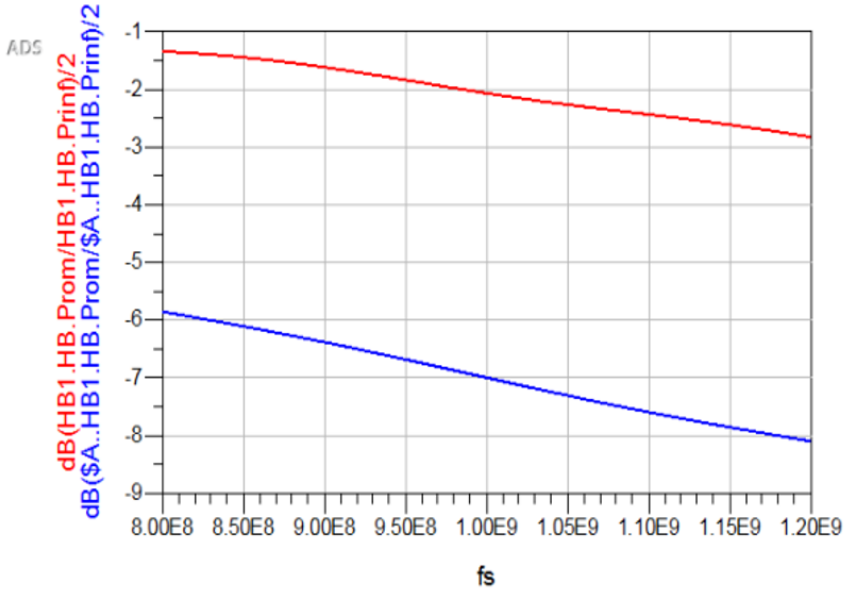

Figure 3.14: Comparison of conversion gain at lower sideband ω_{m-s} of the converted signal; red: with inductor; blue: without inductor

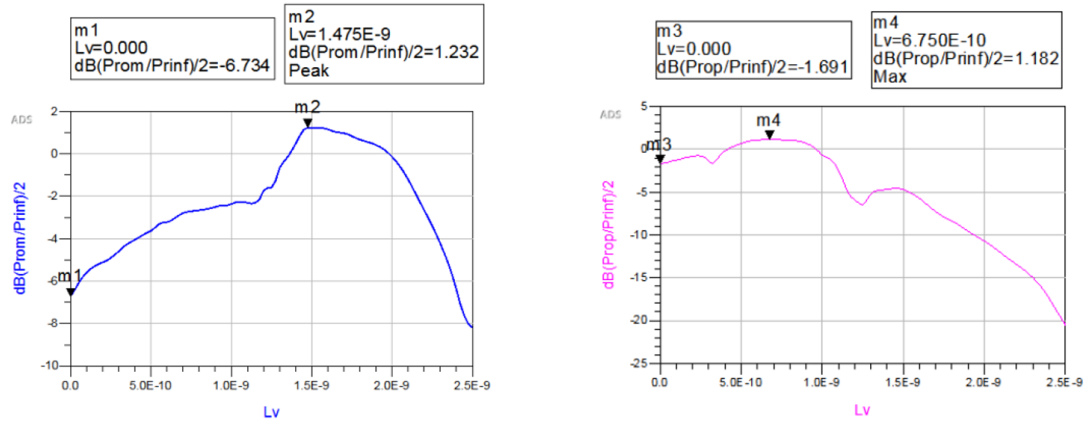

(a) (b)

Figure 3.15: Conversion gain improvement of inductance pump; (a) lower sideband ω_{m-s}; (b) upper sideband ω_{m+s}

In real MMIC design, TVTL was was optimized to have the highest conversion gain at

lower sideband of the converted signal ω_{m-s}, with signal frequencies from 0.8 GHz to 1.2 GHz and carrier frequency at 4.5 GHz. Under such conduction, the upper sideband ω_{m+s} of the converted signals was very likely to be suppressed by the stopband of TVTL. The optimal inductance value was 1.44 nH. Figure 3.16 shows the small-signal performance of the designed TVTL with bias voltage equal to -7 V, where the red line is the return loss of the MMIC TVTL, and the blue line depicts the insertion loss of the designed TVTL. The return loss indicated that the periodic structure was well match to 50 Ω up to 4.5 GHz. The insertion loss showed that the MMIC TVTL had a cutoff frequency at 5 GHz.

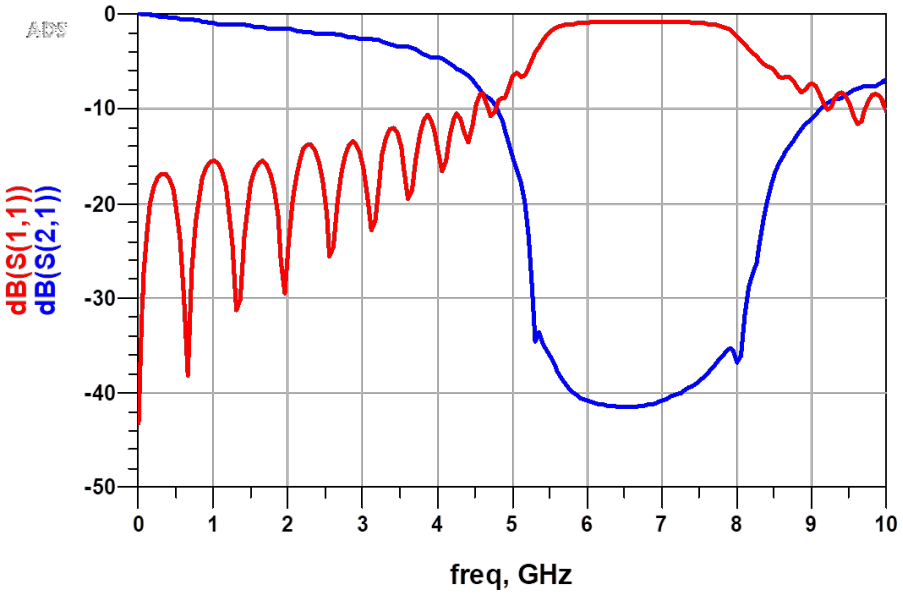

Figure 3.16: Simulated S-parameter of the MMIC TVTL designed for optimal performance at lower sideband; blue: insertion loss of TVTL; red: return loss of TVTL.

It was also observed in Figure 3.17 that the conversion gain of the lower sideband ω_{m-s} of the converted signals was -3.9 dB at 1 GHz, and the conversion gain of the upper sideband at frequency ω_{m+s} of the converted signal was much lower than that of the lower sideband. This was because the converted upper sideband at frequency ω_{m+s} fell into the stopband of the designed structure, so it was mostly suppressed in TVTL as mentioned before. Compared with ideal case, the conversion gain became conversion loss in MMIC design due to the

Ohimic loss from the thin metal layers with finite conductivity, which can be improved with better fabrication process.

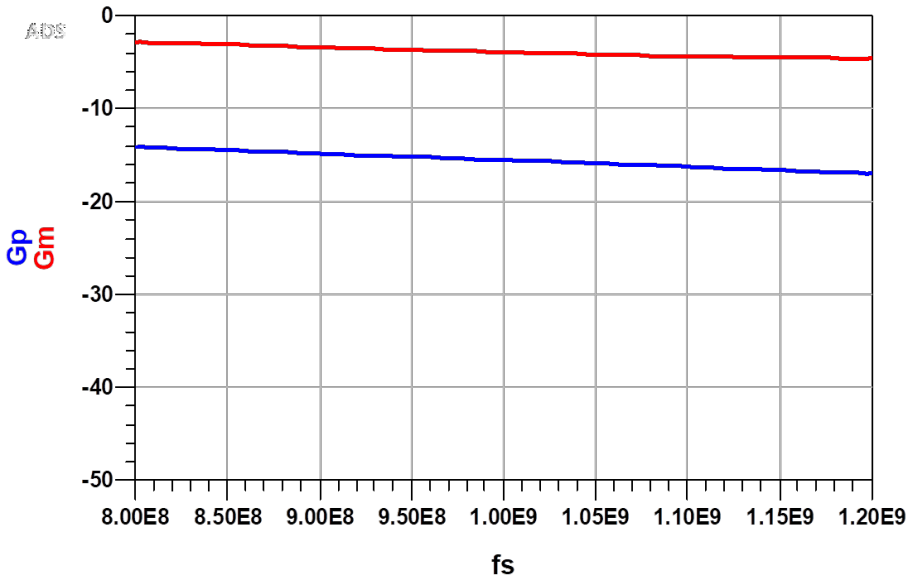

Figure 3.17: Simulated conversion gain of the MMIC TVTL designed for optimal performance at lower sideband; blue: upper sideband ω_{m+s}; red: lower sideband ω_{m-s}.

In addition, as shown in Figure 3.18, the signal gain increased rapidly when frequency was larger than 0.8 GHz. This indicated the beginning of exponential parametric coupling mode. Again, the signal gain became small loss in MMIC design due to the additional resistive loss from the thin microstrip lines. Furthermore, the signal loss stopped to decrease at frequency 1.05 GHz. This was because of the higher Ohmic loss at higher frequencies.

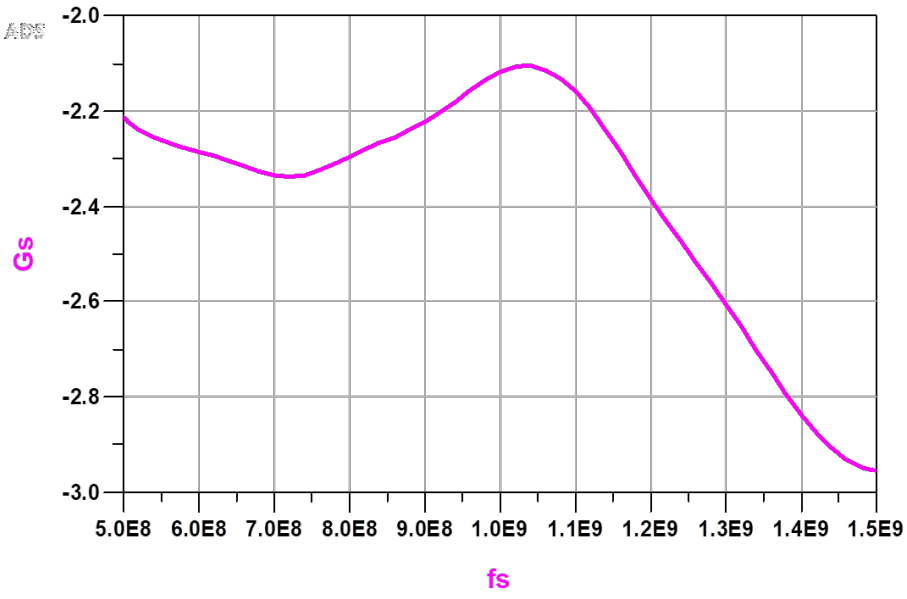

Figure 3.18: Simulated signal of the designed MMIC TVTL.

CHAPTER 4

Performance of Monolithic Integrated Time-varying Transmission Lines (TVTL)

The design and simulation of MMIC TVTLs were discussed in the previous chapter. Several versions of MMIC designs were fabricated with Global Communication Semiconductors, LLC (GCS) 1 μm InGaAs HBT process, on which experiments were performed. Figure 4.1 shows an example of fabricated transmission-line-based MMIC TVTL, where a meander transmission line was periodically loaded with 16 varactor diodes. The size of the chip is 5070 μm $\times$ 5270 μm. The operating signal frequency was designed from 0.5 GHz to 1.5 GHz, with a carrier designed from 4 GHz to 4.5 GHz.

To further reduce chip area, another type of TVTL structure was also employed, in which the meander transmission line in Figure 3.13 was replaced by inductors. This structure was first proposed in [5]. It had the same bahavior as the transmission-line-based TVTL, but it was much smaller than that based on meander transmission line. The diagram of inductor-based TVTL is depicted in Figure 4.2, and one of the fabricated 12-unit inductor-based TVTLs is illustrated in Figure 4.3. The overall size of this chip is 4460 μm $\times$ 1520 μm.

In this chapter, we will go over the experimental setups and measured parametric amplification effects of MMIC TVTLs. Then, two applications of TVTL, namely frequency translational RF receiver and low-loss delay line, will be discussed in Section 4.2.

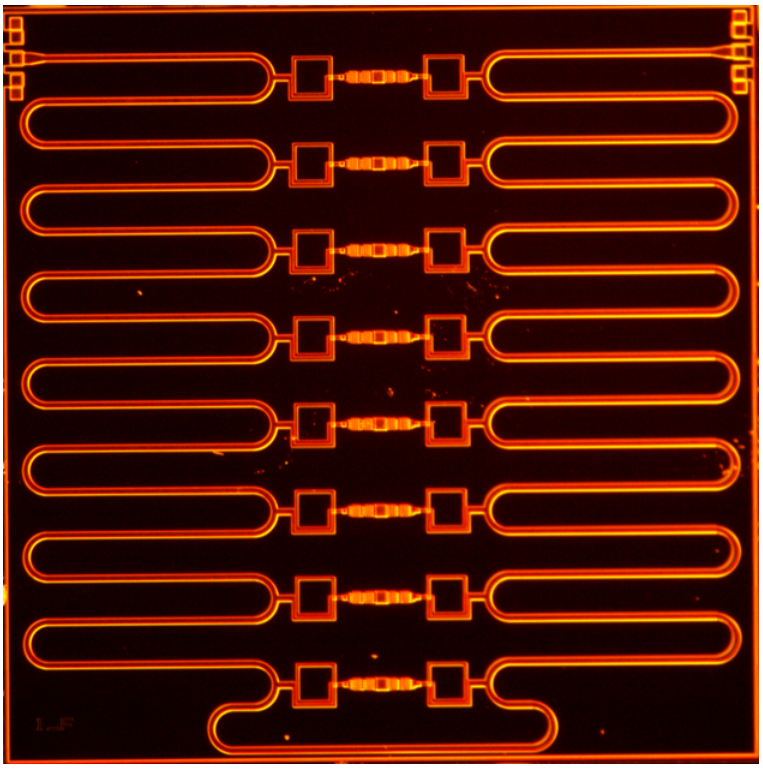

Figure 4.1: 16-unit transmission-line-based MMIC TVTL chip.

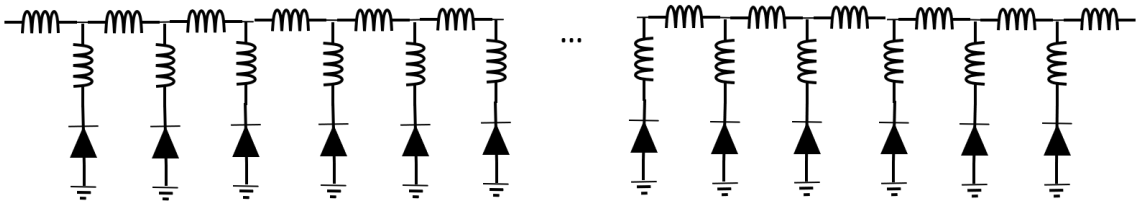

Figure 4.2: Schematic of inductor-based MMIC TVTL

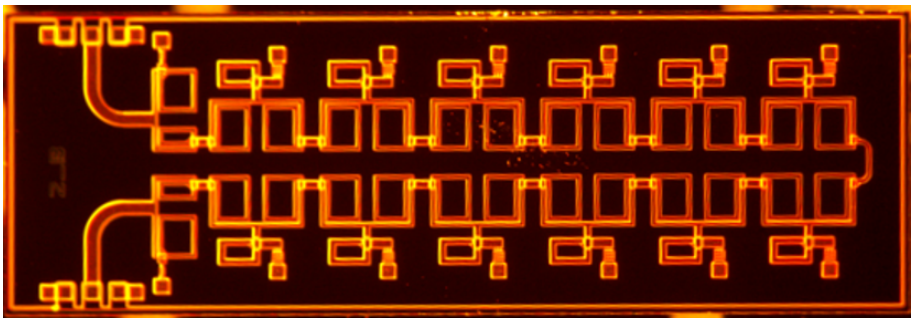

Figure 4.3: 12-unit inductor-based MMIC TVTL chip

4.1 Experimental Resutls of TVTL

4.1.1 Small-signal S-parameter Measurement

For transmission-line-based MMIC TVTL shown in Figure 4.1, it was first mounted on a probe station to measure the small-signal performance using a vector network analyzer. During this test, no carrier power was pumped, and varactor diodes were biased at -6 V. This step was to check the impedance matching and the resistive loss of TVTL.

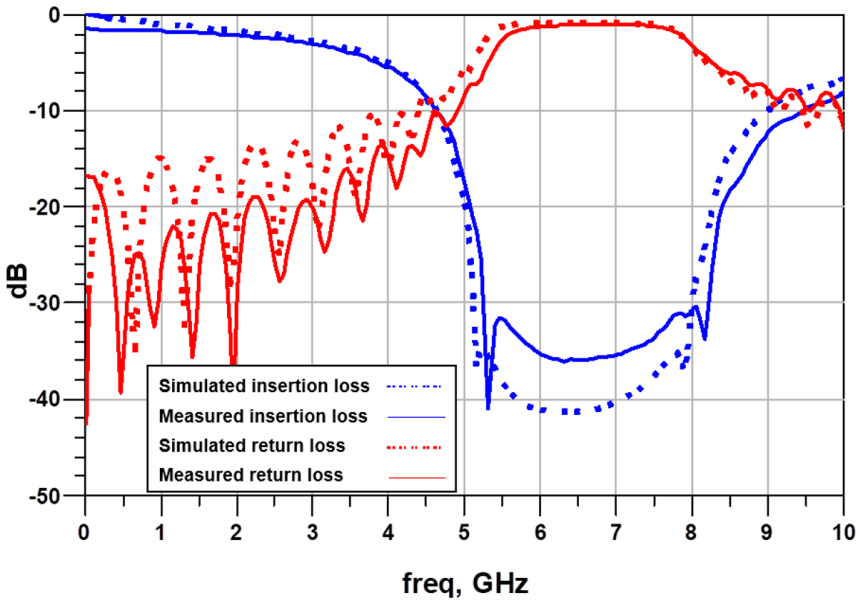

Figure 4.4: Measured and simulated S-parameter of 16-unit MMIC TVTL with diode biased at -6 V; solid lines: measured S-parameter; dot lines: simulated S-parameter.

It can be observed from the measured return loss in Figure 4.4 that transmission-line-based TVTL was well matched to 50 Ω up to 4 GHz, and it agreed with the simulated return loss fairly well except that the passive loss was higher in real circuit. The measured insertion loss in Figure 4.4 indicates that the cutoff frequency of the TVTL was 4.7 GHz under such biasing condition, which matched with the simulated cutoff behavior very well. The cut frequency of TVTL could shift upwards if varactor diodes were biased deeper, and vice versa. Moreover, the resistive loss was much higher than what was predicted by the

simulated results at low frequencies, especially at those below 1 GHz. This might be due to an over-optimistic model in the foundary's design kit.

Similar to transmission-line-based TVTL, small-signal S-parameter measurement was first performed on inductor-based TVTL to verify the impedance matching and evaluate the passive loss of TVTL. The carrier power was turned off during this test, and the bias voltage across varactor diodes were -5 V. As shown in Figure 4.5, this inductor-based TVTL was well matched to 50 Ω up to 6 GHz, and the cutoff frequency was 7 GHz.

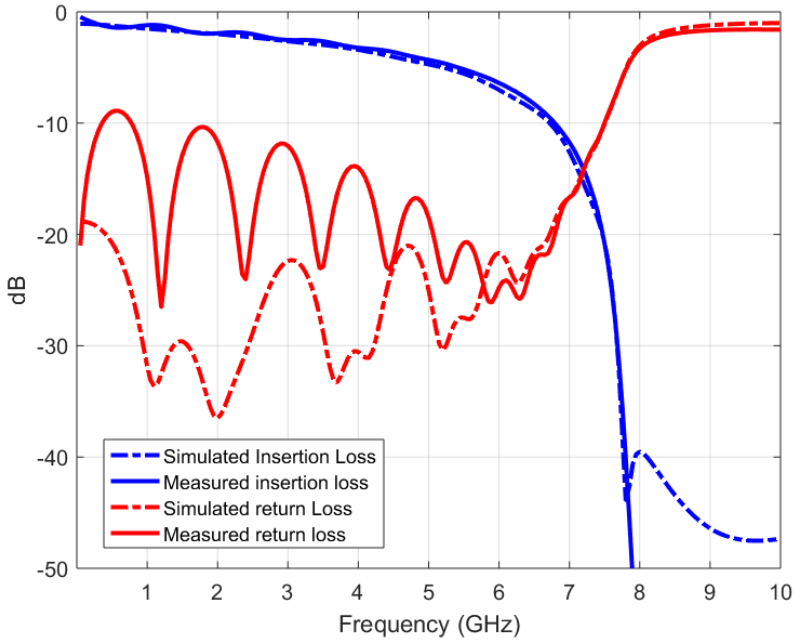

Figure 4.5: Measured and simulated S-parameter of 12-unit inductor-based MMIC TVTL with diode biased at -5 V; solid lines: measured S-parameter; dot lines: simulated S-parameter.

4.1.2 Large-signal Conversion Gain Measurement

After verifying the small-signal performance of transmission-line-based TVTL, a mixer test was performed to examine TVTL's parametric coupling behavior. A Keysight PNA-X was used in this measurement to generate the 0.5 GHz to 1.5 GHz -10 dBm input signals of TVTL. They were then combined with a 33.2 dBm 4.5 GHz carrier by a diplexer. The carrier wave

was generated by an external signal generator and amplified by a power amplifier to the desired power level. After that, the combined RF signal was fed into TVTL through a bias network with negative DC bias. The output of TVTL was connected to another bias network to filter out the DC component. The remaining RF component contained several tones including ω_s, ω_m, ω_{m-s}, so another diplexer was needed to get the desired converted signal at frequency ω_{m-s}. Lastly, this converted tone was analyzed by PNA-X to measure the conversion gain of TVTL. The test setup was first calibrated to the output of VNA cables and then de-embedded to the probe tips. Figure 4.6 illustrates the diagram of the measurement setup.

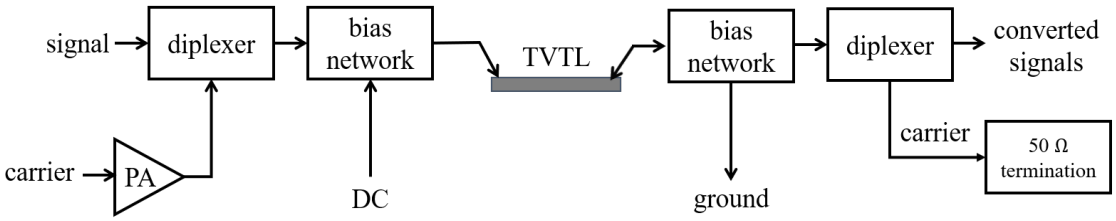

Figure 4.6: Test setup of large-signal conversion gain measurement.

The measured conversion gain between lower sideband at frequencies ω_{m-s} of the converted signal and the original input signal at frequency ω_s is depicted in Figure 4.7. The bias voltages across varactor diodes were swept from -5.5 V to -8.5 V during the test. Small positive gain was observed at frequencies around 600 MHz when a 33.2 dBm carrier power was pumped. The conversion gain gradually increased with the increase of bias voltage. This was due to better quality factors of varactor diodes at deeper bias. Besides, the conversion gain decreased with the increase of signal frequency. This was because of a smaller ratio between β_{m-s} and β_s when signal frequency increased, and the ratio played an important role in conversion gain as indicated by equation (2.16). Noted that the small ripples in the measured results was largely from the mismatch caused by test components such as probes and diplexers.

The conversion gain experiment was also performed on inductor-based TVTL as re-

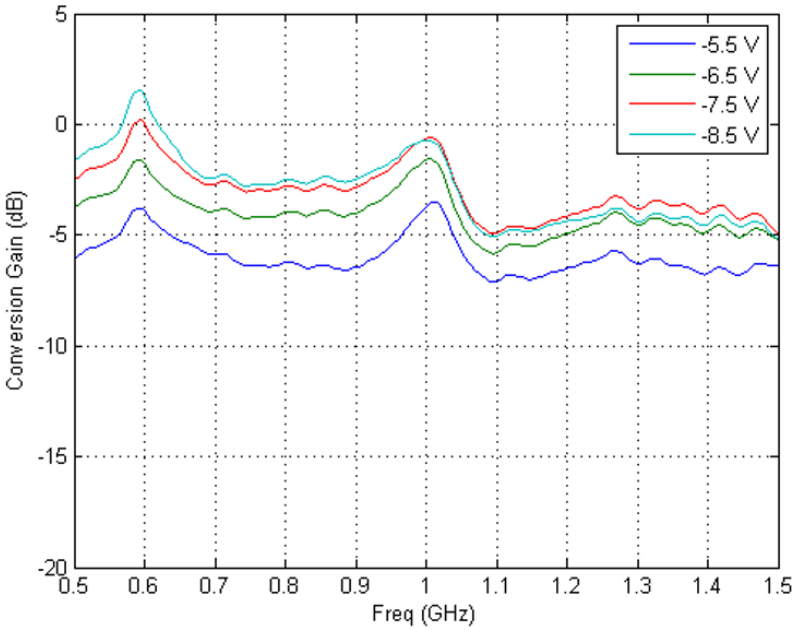

Figure 4.7: Large-signal conversion gain measurement on transmission-line-based MMIC TVTL; bias voltage was swept from -5.5 V to -8.5 V.

ported in [5]. Moderate amout of conversion gain was observed at frequency smaller than 700 MHz, with a 26.9 dBm 4.5 GHz carrier (See Figure 4.8).

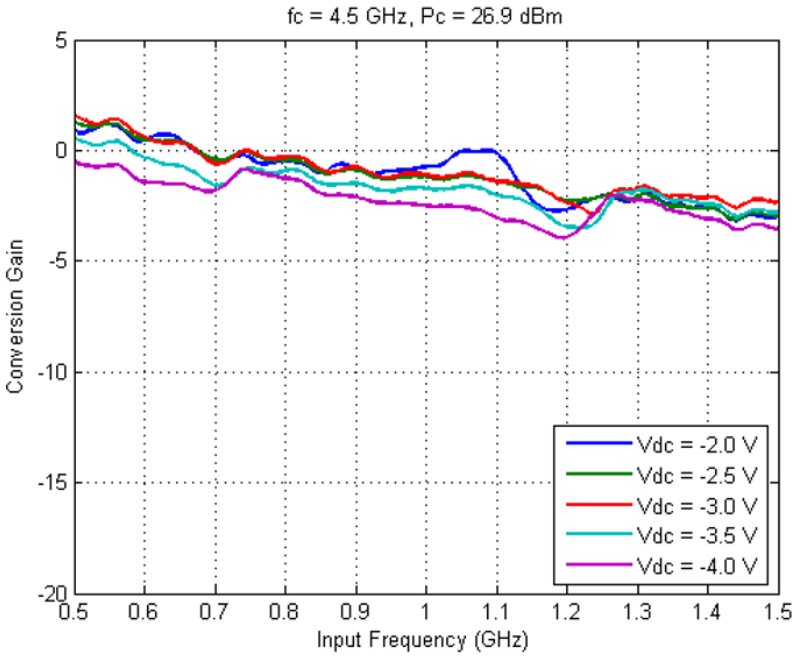

Figure 4.8: Large-signal conversion gain measurement on inductor-based MMIC TVTL; bias voltage was swept from -2.0 V to -4.0 V.

4.1.3 Large-signal Signal Gain Measurement

Then, a signal gain test was performed over the inductor-based MMIC TVTL. The measurement setup was very similiar to the one shown in Figure 4.6 except that the desired output from the second diplexer was signal tone, i.e. ω_s, instead of the lower sideband ω_{m-s} of the converted signals. The diagram of the test setup is shown in Figure 4.9.

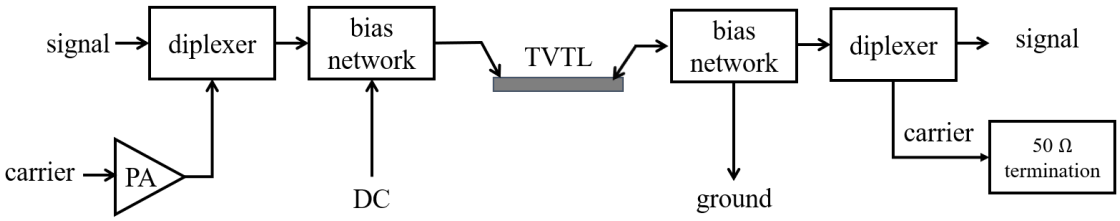

Figure 4.9: Test setup of large-signal signal gain measurement.

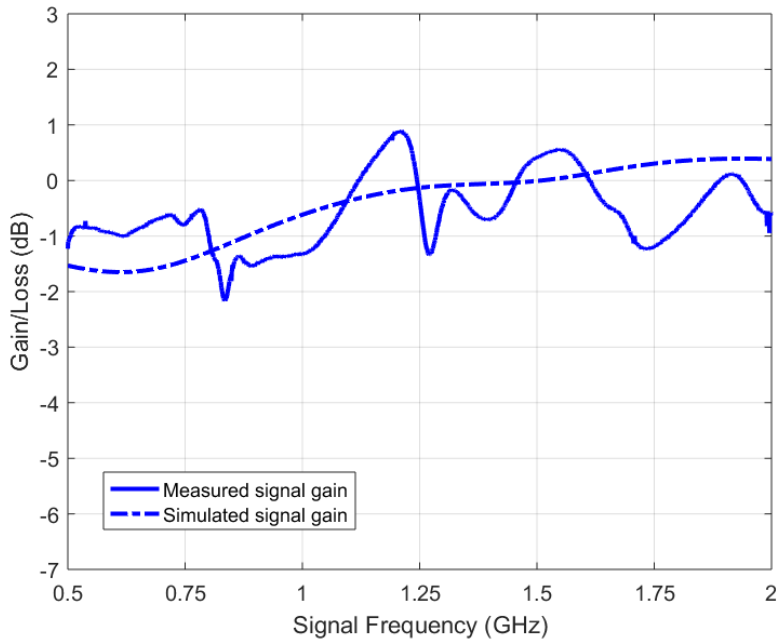

Figure 4.10: Measured and simulated signal gain with diode biased at -5 V; solid line: measured signal gain; dot line: simulated signal gain.

In this test, a -15 dBm of frequency ranging from 0.5 GHz to 2 GHz was chosen and was then combined with a 21.4 dBm 6 GHz carrier as the input to TVTL. After passing

TVTL, the signal tone at frequency ω_s was filtered out by a diplexer with cutoff frequency at 2.3 GHz. As shown in Figure 4.10, the loss at signal frequency ω_s gradually decreased as frequency exceeds 1 GHz. This was because the upper sidband ω_{m+s} of the converted signal fell into the cutoff of TVTL, and TVTL entered exponential parametric mode. The ripples in the measurement was mainly due to mismatches introduced by peripheral componets such as probes and diplexers.

4.2 Applications

4.2.1 Application: Frequency Translational RF Receiver [4, 5]

As discussed in Chapter 2, time-varying transmission lines (TVTL) has uni-directional frequency translation feature. This broadband frequency conversion introduces zero noise theoretically. It can be utilized in a software-defined front-end that is able to select receving band on the fly without using a sharp tunable diplexer. The tunability is enabled by the fact that the converted band after TVTL can be shifted up and down by changing carrier frequency ω_m. Then, a fixed filter with center frequency ω_f can be applied to select the desired received band at frequency $\omega_m - \omega_f$. The concept of frequency translational RF receiver is depicted in Figure 4.11. The first stage of the receiver consists of a TVTL chip and a fixed bandpass filter, where TVTL operates as a parametric mixer. The carrier of TVTL is frequency tunable so that it can make the desired received signal fall into the passband of the fixed bandpass filter while leaving off-band jamming signals rejected. This helps to prevent the saturation of LNA at the second stage caused by the jamming signals from adjacent channels. Moreover, TVTLs may offer zero insertion loss or even small conversion gain over a broad range of frequencies. This helps to minimize the noise figure of the receiver and compensate for the loss introduced by the filter after TVTL as well.

Figure 4.12 shows the measured conversion loss of the proposed structure, in which the fixed bandpass filter had a center frequncy at 3.525 GHz with a 3 dB bandwidth of 50 MHz.

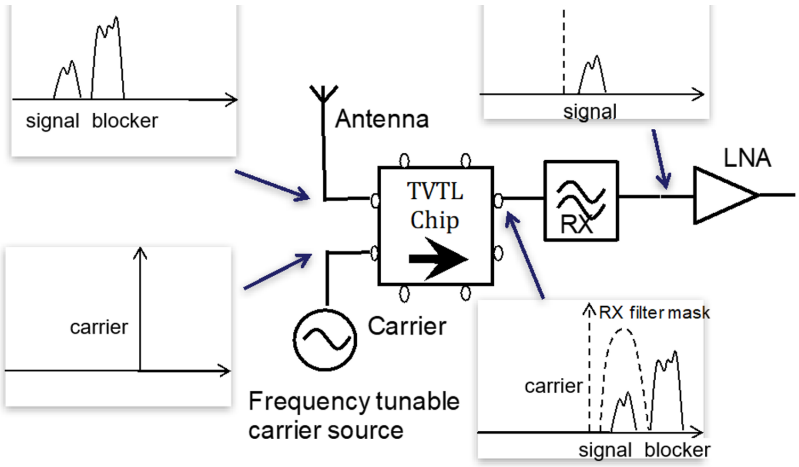

Figure 4.11: Diagram of frequency translational RF receiver.

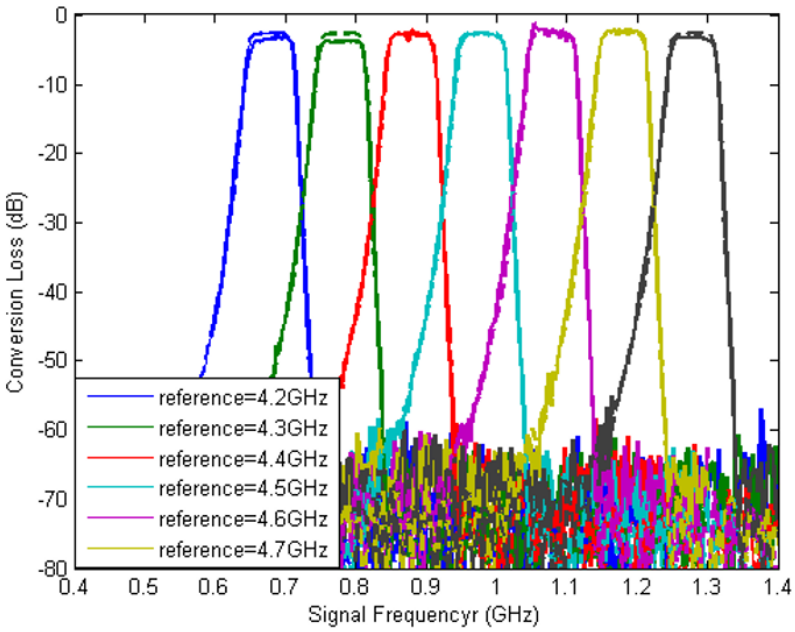

Figure 4.12: Measured conversion loss of the proposed frequency translational RF receiver; solid lines: response of the selected received band at original frequency ω_s; dash lines: frequency shifted version of the insertion loss of bandpass filter as references.

The carrier frequencies varied from 4.2 GHz to 4.8 GHz with a 0.1 GHz step in the test. This corresponded to select the signal frequency from 665 MHz to 1.265 GHz. The minimum conversion loss of the structure including the bandpass filter was 2.8 dB with carrier frequency at 4.4 GHz. Furthermore, the conversion loss in all the cases almost overlapped with the insertion loss of the bandpass filter (as indicated by the dash line in Figure 4.12). In other words, TVTL introduces only small amount of additional loss to the system. Noted that all the measured responses were shifted back to its original frequency manually for better illustration.

The noise figure of the proposed frequency translational RF receiver approached to the conversion loss of the structure. This is similiar to the property of a passive device [4].

4.2.2 Application: Low-loss Delayed Line

As introduced in Chapter 2, time-varying transmission lines (TVTL) can offer exponential parametric coupling when the upper sideband ω_{m+s} of the converted signal is suppressed by the stopband of TVTL. This exponential parametric coupling may provide amplification especially at signal frequency ω_s, so a low-loss delay line without loss or even with small gain can be developed. Figure 4.13 shows the signal gain/loss with and without carrier power pumped in. Noted that without carrier power, TVTL functions exactly as a traditional transmission line. With the help of pumped carrier power that results in time-varying capacitance in the transmission line, a 2.53 dB of insertion loss improvement was observed at 1.2 GHz. The phase delay between input and output increased linearly with signal frequency. More than 360 degrees of delay was obtained for signal with frequency greater than 1.53 GHz, as shown in Figure 4.14.

Moreover, it is well known that the insertion loss of a passive component determines its noise figure. The noise figure degradation is irreversible even if an amplifier is cascaded to boost up the signal power. The exponential parametric amplification provided by TVTL, however, worked differently because signal was being amplified as soon as it entered the

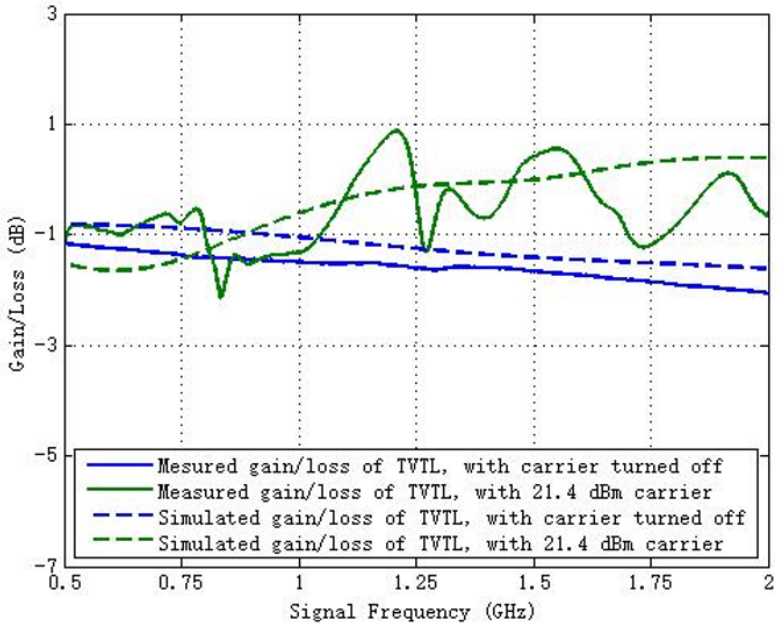

Figure 4.13: Measured and simulated gain/loss of 12-unit MMIC TVTL at the original signal frequency, with varactor diodes biased at -5 V.

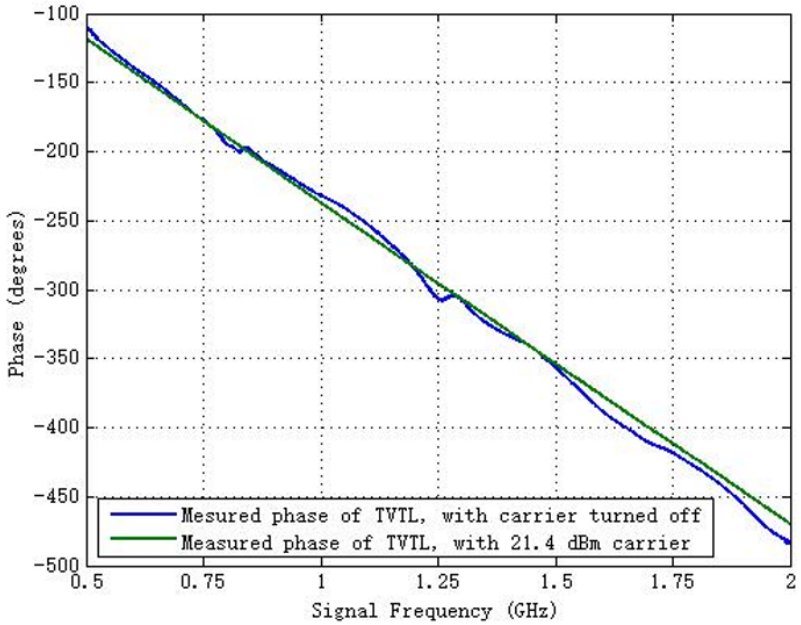

Figure 4.14: Measured phase delay of 12-unit MMIC TVTL at the original frequency, with varactor diodes biased at -5 V.

transmission line. The signal-to-noise ratio (SNR) would not be sacrificed that much. As indicated in Figure 4.15, the noise figure of a classic transmission line, i.e. TVTL without carrier pumped in, was approximately the same as its insertion loss. Furthermore, the noise figure of TVTL was generally better than that of its passive counterpart once it entered exponential parametric amplification region.

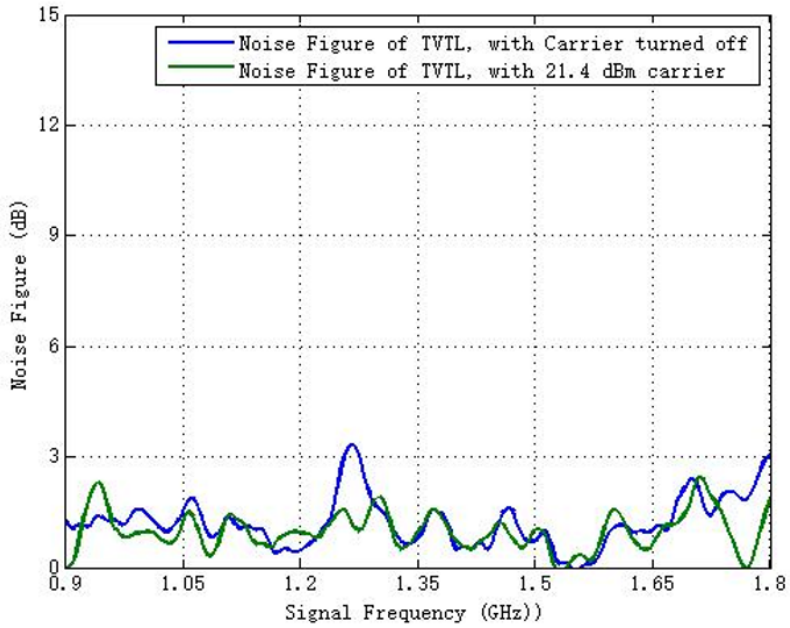

Figure 4.15: Measured noise figure of 12-unit MMIC TVTL, with varactor diodes biased at -5 V.

Therefore, it is possible to apply TVTL as a long-delay, low-loss, and low-noise transmission line on-chip to overcome some performance limits in passive components.

CHAPTER 5

Conclusions

In this thesis, the theoretical analysis of parametric amplification modes of time-varying transmission lines (TVTL) was done in Chapter 2. With three-tone assumption, one can derive equation (2.13) that represents the sinusoidal parametric amplification mode in TVTL. With two-tone assumption, exponential parametric amplification mode is obtained in equation (2.16). These were verified in both ideal TVTL simulations in Chap 3 and MMIC TVTL measurements in Chapter 4.

The noise figure analysis in Section 2.3 indicates that the noise added by TVTL comes mainly from the thermal noise directly emitted at $\omega_{m\pm s}$ by varactor diodes. Moreover, quality factors of varactor diodes and capacitance modulation index play an important role in TVTL's noise figure. Therefore, one should choose varactor diodes with high quality factor and wide linear variation range to reduce noise added by TVTL.

In MMIC TVTL design, measurement-based varactor diode modeling was first carried out. This was to derive an accurate device model to assist TVTL design. With the help of varactor diode model, we can better predict the small-signal behavior of TVTL. After that, TVTL with inductance pump was designed and fabricated. This structure can help reduce carrier power. It can also boost up the capacitance modulation index, and thus leading to a higher conversion gain.

During experiment on MMIC TVTLs, small amount of conversion gain was observed in both transmission-line-based TVTL and inductor-based TVTL. These parametric ampifi-

cation effects can be applied as a parametric mixer in a frequency translation RF receiver that can tackle with adjacent channel interference. Aside from evaluating gain at mixing tones $\omega_{m\pm s}$, signal gain test at ω_s was also performed on a 12-unit inductor-based TVTL, in which a maximum 2.43 dB insertion loss improvement was observed at 1.2 GHz. When TVTL entered exponential parametric amplification region, the noise figure with carrier power pumped in was generally better than that without carrier power. This parametric amplification effect at original frequency ω_s might be applied to design long-delay, low-loss, and low-noise RF delay lines.

References

[1] Shihan Qin, Qiang Xu, and Yuanxun Ethan Wang. Nonreciprocal components with distributedly modulated capacitors. *IEEE Transactions on Microwave Theory and Techniques*, 62(10):2260–2272, 2014.

[2] Shihan Qin and Yuanxun Ethan Wang. Broadband parametric circulator with balanced monolithic integrated distributedly modulated capacitors (DMC). In *Microwave Symposium (IMS), 2016 IEEE MTT-S International*, pages 1–4. IEEE, 2016.

[3] Shihan Qin and Yuanxun Ethan Wang. A nonreciprocal, frequency-tunable notch amplifier based on distributedly modulated capacitors (DMC). In *Microwave Symposium (IMS), 2016 IEEE MTT-S International*, pages 1–3. IEEE, 2016.

[4] Qianteng Wu, Xiating Zou, Shihan Qin, and Yuanxun Ethan Wang. Frequency translational RF receiver with time varying transmission lines (TVTL). In *Microwave Symposium (IMS), 2017 IEEE MTT-S International*, pages 1767–1769. IEEE, 2017.

[5] Qianteng Wu, Xiating Zou, Rui Zhu, and Yuanxun Ethan Wang. Chip-scale RF correlator with monolithically integrated time-varying transmission line (TVTL). In *Microwave Symposium (IMS), 2018 IEEE MTT-S International*. IEEE, 2018.

[6] Andrew J Viterbi and Andrew J Viterbi. *CDMA: principles of spread spectrum communication*, volume 122. Addison-Wesley Reading, MA, 1995.

[7] Ashish Pandharipande. Principles of ofdm. *IEEE potentials*, 21(2):16–19, 2002.

[8] Mikael Gudmundson and P-O Anderson. Adjacent channel interference in an ofdm system. In *Vehicular Technology Conference, 1996. Mobile Technology for the Human Race., IEEE 46th*, volume 2, pages 918–922. IEEE, 1996.

[9] Eduard Garcia Villegas, Elena Lopez-Aguilera, Rafael Vidal, and Josep Paradells. Effect of adjacent-channel interference in ieee 802.11 wlans. In *Cognitive Radio Oriented Wireless Networks and Communications, 2007. CrownCom 2007. 2nd International Conference on*, pages 118–125. IEEE, 2007.

[10] David M Pozar. *Microwave engineering*. John Wiley & Sons, 2009.

[11] PK Tien. Parametric amplification and frequency mixing in propagating circuits. *Journal of Applied Physics*, 29(9):1347–1357, 1958.

[12] A Van der Ziel. On the mixing properties of non-linear condensers. *Journal of Applied Physics*, 19(11):999–1006, 1948.

[13] Rolf Landauer. Shock waves in nonlinear transmission lines and their effect on parametric amplification. *IBM Journal of Research and Development*, 4(4):391–401, 1960.

[14] PK Tien and H Suhl. A traveling-wave ferromagnetic amplifier. *Proceedings of the IRE*, 46(4):700–706, 1958.

[15] Hiroyuki Ito and Kazuya Masuy. A simple through-only de-embedding method for on-wafer s-parameter measurements up to 110 ghz. In *Microwave Symposium Digest, 2008 IEEE MTT-S International*, pages 383–386. IEEE, 2008.